

We are IntechOpen, the world's leading publisher of Open Access books Built by scientists, for scientists

6,900

Open access books available

186,000

International authors and editors

200M

Downloads

Our authors are among the

154

Countries delivered to

TOP 1%

most cited scientists

12.2%

Contributors from top 500 universities



WEB OF SCIENCE™

Selection of our books indexed in the Book Citation Index
in Web of Science™ Core Collection (BKCI)

Interested in publishing with us?
Contact book.department@intechopen.com

Numbers displayed above are based on latest data collected.
For more information visit www.intechopen.com



Manufacturing and Investigating Objective Lens for Ultrahigh Resolution Lithography Facilities

N.I. Chkhalo, A.E. Pestov, N.N. Salashchenko and M.N. Toropov
*Institute for physics of microstructures RAS, GSP-105, Nizhniy Novgorod
Russia*

1. Introduction

Current interest in super-high-resolution optical systems is related to the development of a number of fundamental and applied fields, such as nanophysics and nanotechnology, X-ray microscopy in the «Water window» and the projection nanolithography in the extreme ultraviolet (EUV) spectral range (Gwyn, 1998; Benschop et al., 1999; Naulleau et al., 2002; Ota et al., 2001; Andreev et al., 2000; Cheng, 1987). The great economical importance in applying the EUV lithography which, as expected, should replace the conventional deep ultraviolet lithography in commercial production of integrated circuits with topology at a level of 10-30 nm dictates a level of efforts carried out in the fields related to the technology. In the spectral range of soft X-ray and EUV radiation ($\lambda=1-40$ nm) this interest is accompanied by the intensive development of a technology for depositing highly reflecting multilayer interference structures (MIS) (Underwood & Barbee, 1981). In practice, the requirements for the shape of individual optical components and for the spatial resolution of optical systems are imposed on designing projection extreme ultraviolet lithography setups that operate at a wavelength of 13.5 nm (Williamson, 1995). EUV lithography should replace the conventional deep-ultra-violet lithography at 193-nm-wavelength radiation generated by excimer lasers in the commercial production of integrated circuits with a minimum topological-element size of 10-20 nm.

The paper is devoted to the fundamental problems of manufacturing and testing substrates with fine precision for multilayer mirrors which surface shape, as a rule, is an aspherical one and that should be made with a sub-nanometer precision, to characterizing multilayer covers deposited onto these substrates which should not injure the initial surface shape and also to measuring with the sub-nanometer accuracy the wave-front aberrations of high-aperture optical systems, for instance, projective objectives.

The main requirements for the shape and for the micro-roughness values of substrate surfaces attended to depositing MIS on them which are optimized for maximum reflectivity at a 13.5 nm wavelength are considered. The problem of roughness measurement of atomic-level smooth surfaces is discussed. The application of optical interferometry for characterizing the surface shape and wave-front aberrations of individual optical elements and systems is under consideration. A particular attention has been given to interferometers with a diffraction reference wave. The problem of measurement accuracy provided by the interferometers which first of all are connected with aberrations of the diffracted reference

Source: Lithography, Book edited by: Michael Wang,
ISBN 978-953-307-064-3, pp. 656, February 2010, INTECH, Croatia, downloaded from SCIYO.COM

wave is under discussion. The reference spherical wave source based on a single mode tipped fiber with a sub-wave exit aperture is fully considered. The results of studying this source and the description of an interferometer with a diffraction reference wave made on the base of the source are given. The application of this interferometer for characterizing spherical and aspherical optical surfaces and wave-front aberrations of optical systems is illustrated.

The achieved abilities of the interferometric measuring the surface shape of optical elements with a sub-nanometer accuracy make possible to develop different methods for correcting the optical element surfaces, initially made with traditional for optical industry precision (root-mean-square deviation from the desired one about $RMS \approx 20-30$ nm) to the same sub-nanometer accuracy. Two methods of a thin film depositing and an ion-beam etching through the metallic masks produced on evidence derived from the interferometric measurements, are considered for the surface shape correction of optical elements. The dependences of the etching rate and the dynamics of the surface roughness on the ion energy (neutral in the case of fused silica etching) and the angle of the ions incidence to the corrected surface are presented. The final results obtained when correcting substrates for multilayer imaging optics for a 13.5 nm wavelength are reported.

Much attention is paid to the final stage of a mirror manufacturing and depositing a multilayer interference structure onto the substrate reflecting a short wavelength radiation. Some peculiarities of the deposition technology as applied to the mirrors with ultra-high precision surface shape are discussed. Methods for compensating an intrinsic mechanical stress in the multilayer films developed in IPM RAS are described.

In conclusion, the problems on the way to manufacture atomic smooth ultrahigh precision imaging optics for X-ray and EUV spectral ranges yet to be solved are discussed.

2. The main requirements for the shape and for the micro-roughness of substrate surfaces

According to the Mareshal criterion to achieve the diffraction limited resolution of an optical system it is necessary that a root-mean-square distortion of the system wave front RMS_{obj} must satisfy this ratio (Born & Wolf, 1973)

$$RMS_{obj} \leq \lambda / 14, \quad (1)$$

where λ is a wavelength of light. Since the errors (distortions) of elements of a complex optical system are statistically independent quantities, the required accuracy RMS_1 of manufacturing an individual optical component is

$$RMS_1 \leq \lambda / (14 \cdot \sqrt{N}), \quad (2)$$

where N is a number of components in the optical system. For instance in the case of a six-mirror objective typical of EUV lithography at the wavelength of $\lambda=13.5$ nm, the reasonable error of individual mirror RMS_1 should not exceed 0.4 nm.

Let us consider the influence of objective aberrations on the image quality by the example of imaging of 150 nm width strips by means of Schwarzschild-type objective made up of two aspherical mirrors and providing linear demagnification coefficient of x5, Fig. 1. The calculation was done with the help of ZEMAX code at a wavelength of 13.5 nm. On the left in Fig. 1 a picture of strips to be imaged and their light emission is given.

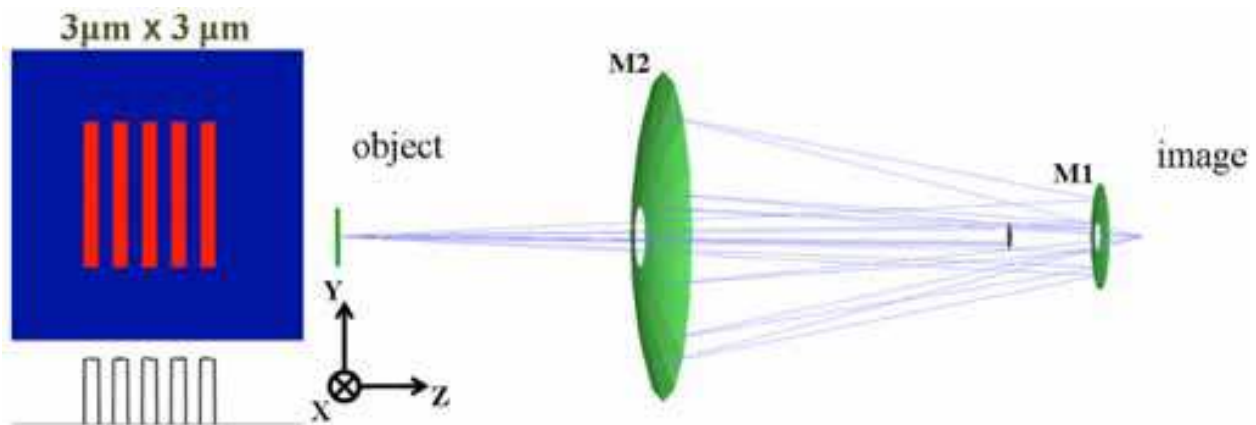


Fig. 1. A projection objective diagram made up of a convex M1 and a concave M2 aspherical mirrors. An exit numerical aperture is $NA=0.3$ and a linear demagnification coefficient is $\times 5$.

The strips images and light intensity distributions in the image plane corresponding to different, from $RMS=\lambda/32$ to $RMS=\lambda/4$, values of the objective wave aberrations are given in Fig. 2. The figure shows that at the aberration of $\lambda/4$ the image has fully disappeared. At $RMS=\lambda/14$ we have the image contrast (ratio of intensities from the minimum to the maximum) at a level of 0.5. At the aberration $RMS<\lambda/24$ the image contrast no longer depends on the aberration and is determined only by a numerical aperture of the objective. In such a manner a reasonable aberration is a value at the level of $RMS\approx\lambda/30$, or 0.45 nm. In view of Eq. (2) the requirements for the quality of individual mirrors are stronger at a level of 0.2 nm.

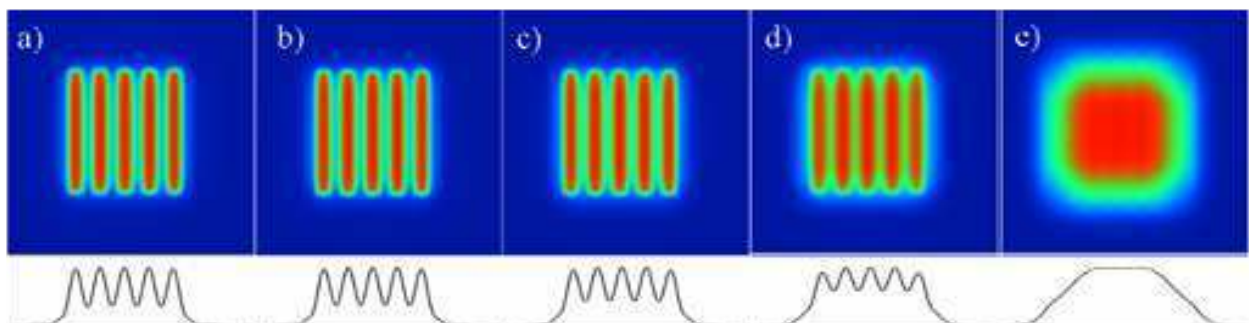


Fig. 2. Images of lines and light intensity distributions in the image plane depending on an objective wave aberration, $\lambda=13.5$ nm. a) - root-mean-square aberration $RMS=\lambda/32$; b) - $RMS=\lambda/24$; c) - $RMS=\lambda/14$; d) - $RMS=\lambda/8$; e) - $RMS=\lambda/4$.

The problem of manufacturing mirrors with a sub nanometer surface shape precision for EUV lithography is complicated by a number of factors. First, because of considerable intensity losses due to the reflection of radiation with a wavelength of $\lambda=13.5$ nm from MIS a number of mirrors in an optical system must be minimized. For this reason to increase a field of view and to achieve a high space resolution of an objective one has to use aspherical surfaces with high numerical apertures. Second, a small radiation wavelength and a huge number of interfaces in multilayer interference structure participating in the reflection process impose rigid requirements on the interfacial roughness, which in turn is substantially determined by the surface roughness of a substrate (Warburton et al., 1987; Barbee, 1981; Chkhalo et al., 1993).

The interfacial roughness with a root-mean-square height σ effects in decreasing both a reflection coefficient of the multilayer mirror and the image contrast because of the scattering of radiation. The estimation of the total integrated scatter (*TIS*) can be done as follows

$$TIS = 1 - \exp\left[-(4\pi\sigma / \lambda)^2\right], \quad (3)$$

where λ is a radiation wavelength. For instance, if the integral scattering of an individual mirror is to be lower than 10%, the interfacial roughness must be at a level $\sigma \leq 0.3$ nm. The more precise analysis shows, that everywhere over the region of space wavelengths of the Fourier transform of the reflecting surface (from fractions of nanometer up to tens of millimeters) the root-mean-square of the surface distortions should be at a level $RMS \leq 0.2$ nm (Williamson, 1995; Sweeney et al., 1998; Soufli et al., 2001).

3. Surface roughness measurement methods

As is seen from ratio (3) among the factors having effect on reflection coefficients of MIS, a substrate surface roughness plays a significant role. There exist a few methods for surface roughness measurements with heights of nanometer and sub-nanometer level at present. Among them the atomic force microscopy (Griffith & Grigg, 1993) and diffusion scattering of hard X-ray radiation (Sinha et al., 1988; Asadchikov et al., 1998) are mostly developed and widely used. A number of papers report a good agreement of experimental data about the surface roughness obtained by both methods (Kozhevnikov et al., 1999; Stone et al., 1999). It is necessary to mention a recently well-established method of a surface roughness measurement by means of an optical interference microscopy (Blunt, 2006; Chkhalo et al., 2008). In this case the producers of the micro interferometers and opticians who use these instruments, report about roughness measurement precision up to 0.01 nm. In particular it is stated that super-polished quartz substrates produced by General Optics (USA) have the roughness at a level of 0.07 nm (Website GO, 2009). But relatively low lateral resolution characteristics of the methods substantially limit the spectrum of space frequencies of a surface roughness to be registered from the high-frequency side, that impairs their capabilities when measuring super-polished substrates attended for short-wavelength optics. For instance, in Fig. 3, where the angular dependence of a scattered intensity of X-ray radiation with a wavelength of $\lambda=0.154$ nm from a fused silica super-polished substrate is presented, one can see that at the angle about 0.6° the scattered intensity is about 10^{-6} of the incident one, down to a detector noise. For the X-rays with $\lambda=0.154$ nm the angle 0.6° corresponds to the scattering on surface space frequencies with a wavelength of $2.8 \mu\text{m}$. This resolution is comparable with the lateral resolution of the interference microscopes and ranks below the resolution of atomic force microscopes. Therefore, noted in some papers a good agreement of experimental data about the surface roughness obtained by these methods can be explained only as follows. In spite on the fact that the radius of a cantilever of the atomic-force microscope may be at the level of a few tens of nanometers, there exist some other factors, such as the true radius of a probe, the peculiarities of the probe moving, vibrations, mathematic processing of experimental data and others, which are specific for each instrument, for each laboratory which decrease the instrumental lateral resolution.

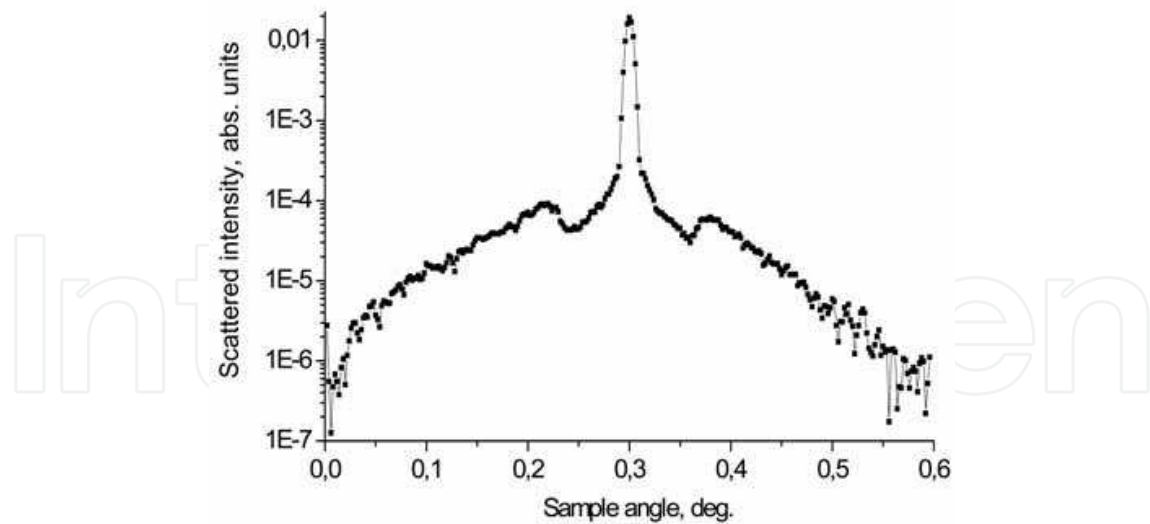


Fig. 3. An angular dependence of scattered intensity of X-ray radiation from a fused silica substrate taken with X-ray diffractometer Philips'Expert Pro at a wavelength of $\lambda=0.154$ nm. Detector angle is fixed $\theta_d=0.6^\circ$.

The most reliable data about the roughness of atomic-smooth surfaces, as we assume, give a method based on the analysis of angular dependencies of specular reflection coefficients of X-ray radiation. The method was proposed in (Parratt, 1954) and was widely used in Refs. (Chkhalo et al., 1995; Protopopov et al., 1999; Bibishkin et al., 2003). The influence of the roughness σ on the angular dependence of the reflection coefficient $R(\theta)$ was taking into account with the help of attenuation coefficient of Nevot-Croce (Nevot & Croce, 1980) as follows

$$R(\vartheta) = R_{id}(\vartheta) \cdot \exp \left\{ -\frac{16\pi^2\sigma^2}{\lambda^2} \cdot \sin \vartheta \cdot \operatorname{Re} \sqrt{\sin^2 \vartheta + \chi} \right\}, \quad (4)$$

where $R_{id}(\theta)$ is an angular dependence of the reflection coefficient on the ideal surface and is calculated with the Fresnel's formulae, λ is a radiation wavelength and χ is a dielectric susceptibility of the substrate material. In the calculations the material optical constants were taken from (Palik, 1985). The advantages of this method are of a "small" size of the probe, the radiation wavelength is comparable with the roughness value, and the lack of limitation about the registered spectrum of space frequencies of a surface roughness from the high-frequency side because in "zero" order of diffraction all radiation losses are taking into account. From middle-frequency side the registered spectrum is limited by the width of the detector slit and is about 30 μm . But it is not the principal restriction since in this range the interference microscopes operate well.

An example of applying this method for the characterization of a fused silica substrate produced by General Optics (USA) in 2007 with a factory specified roughness value of 0.08 nm is given in Fig. 4. As one can see the best fit of the experimental curve (dots) is observed for the surface roughness lying in the range of $\sigma = 0.3\text{--}0.4$ nm. That is 4-5 times more as compared with the specified value. Exactly the same experimental data were obtained in independent measurements made in Institute of crystallography, Russian academy of sciences, in Moscow.

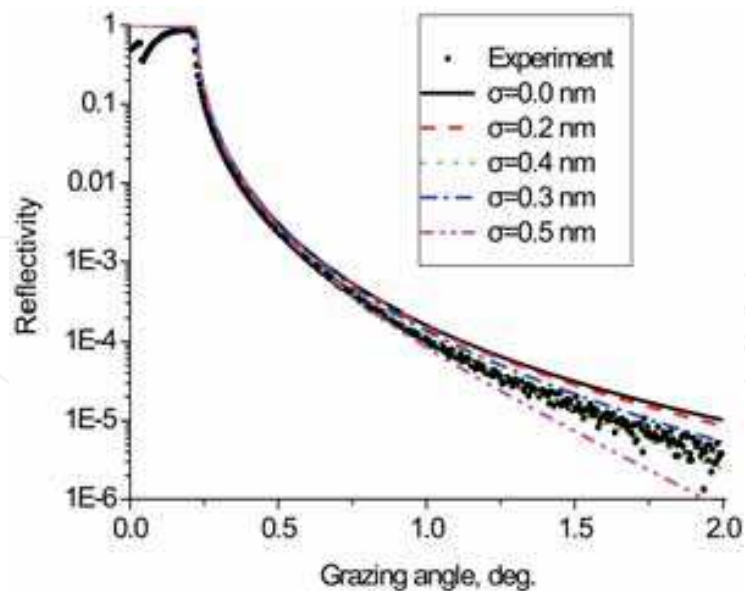


Fig. 4. Angular dependencies of reflection coefficients of radiation with $\lambda=0.154$ nm from a fused silica substrate made by General Optics: dots correspond to experiment; solid lines are calculations corresponding to different roughness values.

The investigation of this substrate by means of an atomic-force microscopy carried out in our institute has shown a strong dependence of measured roughness on the probe size. When we use Si-cantilever the measured roughness was about 0.08 nm, but with a wicker the value has increased up to 0.16 nm. So this direct comparison of the application of X-ray reflection and atomic force microscopy for atomic-smooth surface roughness measurement indicates that the latter method gives an underestimated value of the roughness.

A serious disadvantage of the specular X-ray reflection method is that it allows studying only flat samples while components of imaging optics have concave and convex surface shapes. Therefore, in practice for evaluating the surface roughness of nonplanar samples it makes sense to use the atomic force microscopy method taking into account the calibration of X-ray reflection made with flat substrates.

In conclusion it should be noted that a large body of research done with the help of the x-ray specular reflection method to measure a surface roughness showed that a number of substrates fabricated in different countries had a minimal surface roughness 0.2-0.3 nm and included crystal silicon used in electronic industry. The minimal surface roughness of fused quartz substrates were in the range of 0.3-0.4 nm, except for the case (Chkhalo, 1995), where the roughness of 0.25 nm is reported.

4. Investigating the surface shape by means of optical interferometry

Optical interferometry is one of the most powerful and widely used method for measuring a surface shape of optical components and wave front aberrations of complex systems in the industry. The main advantages of the interferometry are the simplicity and high accuracy of the measurements. The investigation technique is based on the analysis of a light intensity distribution over interference patterns. In this paragraph the basic principles of a surface shape and wave front distortions of optical component and system reconstruction with the use of data obtained by optical interferometers are described. Both types of interferometers

are considered, conventional, utilizing reference surfaces, and diffraction, using as a reference a spherical wave appeared due to the diffraction of light on a wave-sized pin-hole.

4.1 Shape reconstruction and interferometry utilizing reference surfaces

At present a gamma of interferometers is used in an optical industry, including Fizeau and Twyman-Green interferometers which stand out because of their simplicity in operation, high accuracy and universality, is developed. A detailed description of these instruments can be found in many books, for instance (Malacara, 1992; Okatov, 2004). Independently on an optical scheme in this type of instruments the interference patterns are detected which appear as a result of the interaction of two waves, reflected from studied E_S (a surface with defects in Fig. 5) and from reference E_R (top surface in Fig. 5) surfaces. As a result the fringes

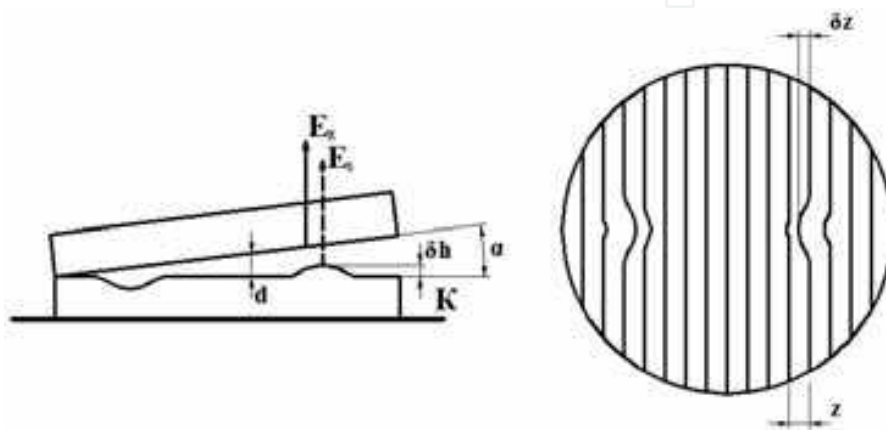


Fig. 5. A fringe pattern formation by interfering of two waves reflected from a surface under study (bottom) and a reference (upper) one.

of so called “equal thickness” are observed. A defect on the surface under study marked in Fig. 5 by symbol z with a height of δh gave rise the phase shift of the reflected light according to

$$\Delta = 2\pi \cdot 2\delta h / \lambda, \quad (5)$$

where λ is a wavelength. The corresponding fringe banding δz , induced by the deviation of the studied surface from the reference can be found from the ratio

$$\delta h = (\lambda / 2) \cdot \delta z / z. \quad (6)$$

These expressions in particular allow to see that the defect with the height of $\lambda/2$ corresponds to one fringe in the interference pattern. When the defects on the studied surface are absent, the fringes make a system of equidistant straight lines. In such a manner the interference pattern uniquely determines the local shape deviations of the surface under study from the reference. So the task of the surface shape reconstruction needs looking for a mathematical model which will fit the experimental data the best.

$$W(x, y) = \Delta h(x, y), \quad (7)$$

where $\Delta h(x, y)$ is the surface deformation in respect to the reference and being a function of coordinates on the surface, $x, y \in \Omega$, Ω is an operating range of the surface. As a rule, the

sought-for function (Braat, 1987) is written in terms of some basis of functions and its description reduces to finding a set of the series coefficients c_k

$$W(\mathbf{r}) = \sum_k c_k \alpha_k(\mathbf{r}), \quad (8)$$

where \mathbf{r} is a radius-vector of a point on the surface and $\alpha_k(\mathbf{r})$ is a set of basis functions. Mostly common polynomials orthogonal on some area Ω_0 are chosen as the basis. For instance, for the circular area these are Zernike polynomials which are widely used in optics (Rodionov, 1974; Golberg, 2001). The orthogonality of the polynomials results in the fact that each term of the series makes a contribution independent on the remaining terms into the mean-square of the wave front deformation.

Since the representation of the investigated function is global any local dilatation when approximating is smoothed thus distorting global view of the function. Besides when reconstructing the surface shape it is important to evaluate not only the global surface shape, but local errors too. From this it follows that the mathematical model should be oriented on the description of the surface shape not only globally, but locally too.

In the framework of this paper this dilemma was solved by introducing local deformations additionally to the global description (8) of the surface deformation function:

$$W(\mathbf{r}) = \sum_k c_k \alpha_k(\mathbf{r}) + \sum_m \left[\sum_j c_{mj} \cdot \beta_j(\mathbf{r} - \mathbf{r}_{0m}) \right], \quad (9)$$

where c_{mj} and β_j are coefficients and "special" basis functions describe a m -th local deformation with the center in the point with the coordinate of \mathbf{r}_{0m} . It is significant that the set of functions $\alpha_k(\mathbf{r})$ and $\beta_j(\mathbf{r} - \mathbf{r}_{0m})$ are different in general case because the described function $W(\mathbf{r})$ should not be interrupted in the range of definition. It is the reason why the "special" functions $\beta_j(\mathbf{r} - \mathbf{r}_{0m})$ must be finite, should not have discontinuity and their values at the definition range boundary must be equivalent to zero. An algorithm of searching for the expansion coefficients of the surface model (9) was performed in two stages. At the first stage the global surface shape error is approximated according to the (8) model. At the second stage the residual local surface deformations are approximated by the right part of the expression (9).

In our case the global description of the surface shape errors is performed with the help of Zernike polynomials $W_Z(\rho, \varphi)$ and the residual local dilatations - by using the apparatus of local splines $W_S(\rho, \varphi)$, which advantages when describing the optical surface deformations are analyzed in (Archer, 1997; Sun et al., 1998) in details:

$$W(\rho, \varphi) = W_Z(\rho, \varphi) + W_S(\rho, \varphi) = \sum_{n=0}^{P_z} \sum_{m=0}^n c_{nm} R_n^m(\rho) \cos(m\varphi) + \sum_{n=0}^{P_z} \sum_{m=0}^n s_{nm} R_n^m(\rho) \sin(m\varphi) + \sum_{i=0}^k \sum_{j=0}^k B_{i,p_s}(\rho \cdot \sin(\varphi)) \cdot B_{j,p_s}(\rho \cdot \cos(\varphi)) P_{ij} \quad (10)$$

where ρ and φ are polar coordinates of the point on the surface, c_{nm} and s_{nm} are the expansion coefficients, $R_n^m(\rho)$, are radial Zernike polynomials, B_{i,p_s} is the basic function of the B-spline of the order of p_s on i -th interval of y coordinate and B_{j,p_s} - is the basic function of the B-spline of the order of p_s on j -th interval of x coordinate and P_{ij} corresponds to the

points of control of the spline. A number of works (Rodionov, 1995; Swantner & Weng, 1994) are devoted to the methods for determining the coefficients of the mathematical model of the surface shape deformation function (10) by using interferometric data. In present work algorithms and programs developed in (Gavrilin, 2003) are used.

Currently available methods of digital registration and mathematical processing of interferograms allow reconstructing the surface shape (wave front aberrations) in respect to the reference surface, Fig. 5, with the accuracy up to $\lambda/10000$, where λ is an operating wavelength of the interferometer. However, the guaranteed surface shape accuracy of the reference in the root-mean-square (RMS) does not exceed $\lambda/30 - \lambda/20$ (Website Zygo, 2009) that is two orders of magnitude worse than required, for instance, for projection nanolithography optics.

A substantially better situation is observed when studying surfaces at typical scales lower than 1 mm. At these scales the accuracy of the reference surfaces is better than $\lambda/1000$ that allows measuring the surface shape deformations with the sub-nanometer accuracy. On this basis a number of micro-interferometers with a digital fringe registration has been developed in the last few years (Blunt, 2006; Chkhalo et al., 2008; Website Veeco, 2009; Website Zygo, 2009). Below the spectrum of space wavelengths on the surface under study to be registered and where the surface shape measuring by interferometers with the sub-nanometer accuracy is limited by the lateral resolution of a microscope is given typically lies in the range of 0.3-1 μm .

4.2 Interferometers with a diffraction reference wave

The problem of conventional interferometers using the reference surfaces is solved by the application of interferometers with a diffraction wave as the reference proposed by V.P. Linnik in 1933 (Linnik, 1933). The proposal is based on the theoretical fact, that when a flat electromagnetic wave falls onto a pin-hole with a diameter comparable with a wavelength in an opaque screen, consisting of a zero-thickness superconducting material, diffracted behind the screen wave in a far wave zone is an "ideal" sphere (Born & Wolf, 1973). This feature of the light diffraction was used as the basis for developing interferometers of this type.

The first interferometer attended to the investigation of optics with sub-nanometer accuracy for the EUV nanolithography has been made by G.E. Sommargren in 1996. As a source of the reference spherical wave he used a single-mode optical fiber with a core diameter (exit aperture) of about 4-5 μm . The objective for a projection scheme of a EUV-nanolithographer was tested with the help of the interferometer (Sommargren, 1996). The author evaluated the measurement precision in terms of the RMS at the level of 0.5 nm. With a high-coherence laser the interferometer allowed testing a surface shape of individual optical elements. The main disadvantage of the interferometer was a "big" source size. A numerical aperture where the diffracted wave still remains "an ideal sphere" is determined by expression $NA_{ref} < \lambda/d$ and in the case of $\lambda=0.5 \mu\text{m}$ and $d=5 \mu\text{m}$ corresponds to $NA_{ref} < 0.1$. Partly the low-aperture problem is solved at the expense of stitching measured data over different areas of the studied substrate or objective. Along with the apparent loss of a measurement accuracy when using the stitching procedure, there exists one even more serious disadvantage of using low-aperture interferometers associated with a strong irregularity of interferogram illumination. Fig. 6 demonstrates how the illumination irregularity results in error when determining the position of the fringe extremum. In other words, along with the apparent

loss of measurement accuracy connected with the stitching, low-aperture interferometers have a significant systematic error induced by strong intensity anisotropy of the reference wave. Therefore, the recent trends are toward increasing the use of diffraction on man-made pin-holes in an opaque screen. Modern microelectronic technologies provide manufacturing high-quality, low-edge roughness pin-holes with diameters down to 40-50 nm.

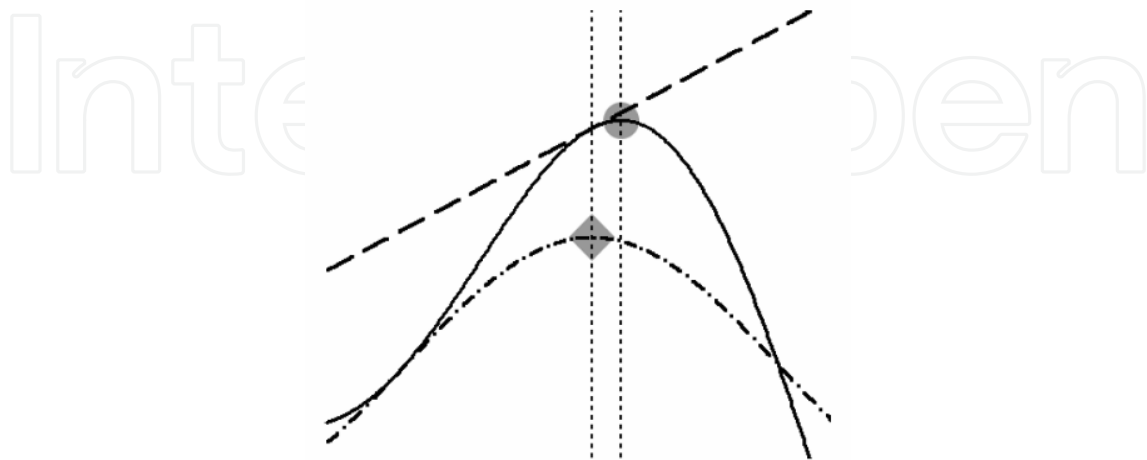


Fig. 6. Shift of determined position of fringe maximum (systematic error) caused by the illumination irregularity.

Such pin-holes are applied in diffraction interferometers operating at the working wavelength of a EUV nano-lithographer, $\lambda=13.5$ nm, which are installed on undulators of the last generation synchrotrons in USA and Japan (Naulleau et al., 2000; Murakami et al., 2003). An interferometer circuit installed on ALS (Berkeley, USA) is given in Fig. 7.

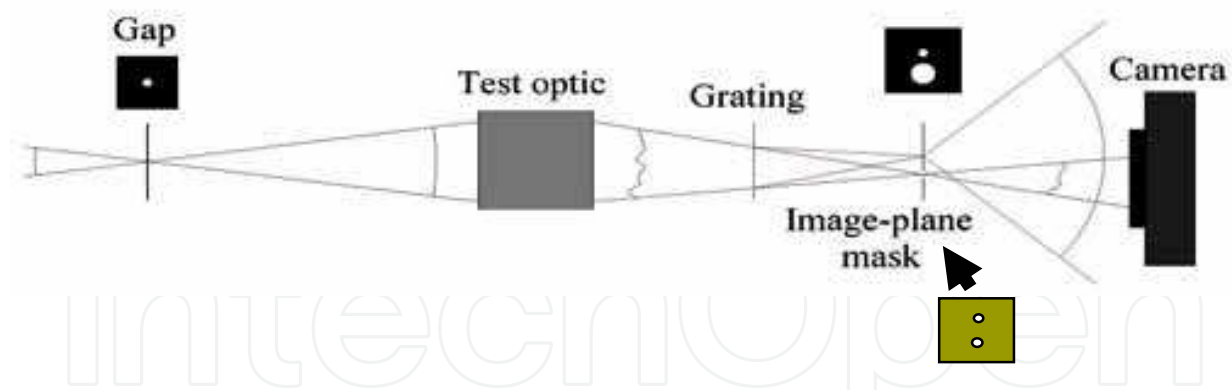


Fig. 7. Optical scheme of interferometer with diffraction reference wave installed on synchrotron ALS in Berkeley, USA. The picture is taken from (Meddecki et al., 1996).

The device operates in the following way. The radiation falls onto a small pin-hole Gap, installed on the lens object plane under study. A diffracted “ideal” spherical wave passing through the lens is distorted according to its aberrations and is collected in the image plane. On the radiation way in-between the lens and the image plane a diffraction grating is installed which splits the wave-front into two ones corresponding to zero and to 1-st diffraction orders. The zero-order radiation passes through the hole which diameter is big enough and exceeds a focusing spot thus preventing the distortion of the wave front. The 1-st order beam is focused onto a small-size pin-hole. Due to the diffraction behind the

screen “an ideal” spherical wave is generated. The reference wave expands toward a CCD-camera where it interferes with a wave passed through the lens under test. The measurement accuracy provided by the interferometer will be discussed later when comparing with our interferometer.

As we can see such interferometers are efficiently used for the final characterization of wave-front aberrations of objectives for EUV radiation. At manufacturing stages of substrates and mirrors the producers of the optics usually use optical diffraction interferometers. The experimental study of capabilities of point diffraction interferometers operating with a visible light has demonstrated a number of factors reducing the measurement accuracy. Particularly systematic discrepancy of experimental data when studying the same optics with the help of visible and EUV light interferometers is observed (Goldberg et al., 2002). All of this stimulated to study the way how finite conductance and thickness of the screen material have an effect on amplitude-phase characteristics of the diffracted wave behind the screen and, correspondingly, on the interferometer measurement accuracy.

In work (Chkhalo et al., 2008) the calculations of the amplitude-phase characteristics of the diffracted field behind the screen in the far-field zone have been carried out. They used the solution of a task about the field of a point source located above a half-space with arbitrary properties and covered with a film of any thickness and arbitrary optical constants given in (Dorofeyev et al., 2003). Fig. 8 illustrates the statement of the problem. The diffraction of a flat wave on a circular hole with the radius of a in a film with thickness of h_f and the inductivity of ε_f in medias with parameters ε and ε_1 was considered. The field was calculated behind the screen at $Z > 0$ on a spherical surface with a fixed radius $R_0 = 10$ cm. The radius R_0 was chosen from practical reasons, but its value does not produce any effect on the community of the result since the calculation was done for a case $kr \gg 1$, where $k = 2\pi/\lambda$ is a wave vector of the diffracted wave in a point with the radius-vector r .

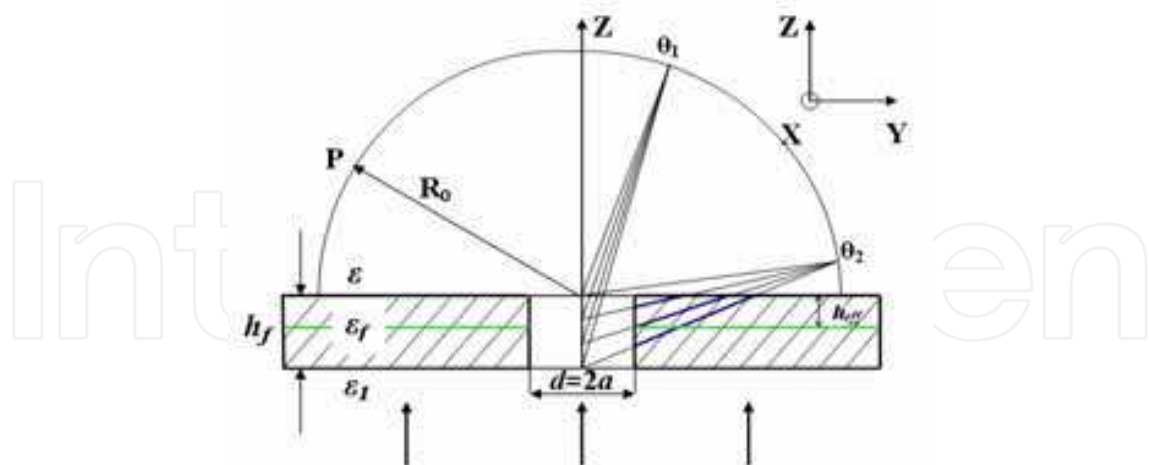


Fig. 8. Sketch of the geometry of the problem, where h_f is the thickness of the film, h_{eff} is an effective film thickness (characterized by the skin-layer), d is the diameter of a hole, ε , ε_1 and ε_f are the dielectric constants of the film and the medias, θ_1 and θ_2 are the angles of diffraction. Incident wave is schematically shown by the arrows.

The results of the calculations as compared with the solution of classical task of diffraction on zero-thickness superconducting screen have shown that most real electro-dynamical

characteristics of the screen material have an effect on phase characteristics of the diffracted field. The calculation of the phase distortions was carried out for the films of aluminum, molybdenum, tungsten and a number of other materials.

The results of numerical calculations shown in Fig. 9 represent a relative phase deviation on meridional angle of the diffracted scalar field in the case of aluminum different thickness films characterized by dielectric constant $\varepsilon_{Al} \approx -54.2 - i21.8$ at the wavelength 633 nm, as compared with the case of a perfect screen $|\varepsilon_{Al}| \rightarrow \infty$. The phase incursion $\Delta\varphi(\theta)$ is expressed in nanometers. The radius of the hole in the films was $a=150$ nm. A case of free standing ($\varepsilon=\varepsilon_1=1$) films was considered. It is evident that the larger the meridional angle, the larger is the phase deviation of the diffracted field in the case of a realistic screen. We connect the result with an additional phase accumulation due to the field propagation through the real film at larger meridional angles (see Fig. 8 for a qualitative clarification). We did not find a thickness dependence on the phase accumulation in the range of $\delta < h_f < 1000$ nm, where δ is a skin-layer, because the phase can be effectively accumulated only inside the skin-layer. The transitions $h_f \rightarrow 0$ and $|\varepsilon_{Al}| \rightarrow \infty$, $|\varepsilon_{Al}| \rightarrow \infty$, or $h_f \rightarrow 0$ led to the known textbook examples. The corresponding diffraction fields for such idealized problems perfectly coincide with those of a spherical phase front.

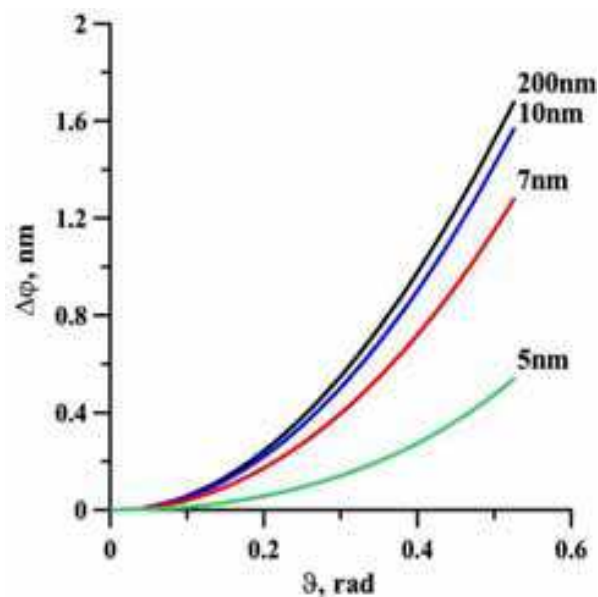


Fig. 9. A relative phase deviation $\Delta\varphi(\theta) = (\varphi(0) - \varphi(\theta)) \cdot \lambda / 2\pi$ on meridional angle of the diffracted field in a case of Al different thickness film ($\varepsilon_{Al} \approx -54.2 - i21.8$) at the wavelength 633 nm on a spherical surface $R_0=10$ cm, the hole radius is $a=150$ nm.

Other mechanisms of the phase distortion can be associated with the excitation of waveguide and surface modes in a plane layer and with a diffraction of such modes by a hole followed by their radiative decay. Since the dielectric constant of all materials in soft X-ray and EUV ranges are close to unity, $Re(\varepsilon) \approx 1$, corresponding phase distortions are minimal. It is one of the reasons why the quality of the diffracted reference wave in EUV region has a better result in a higher measurement precision.

The carried out calculations have shown (see Fig. 10) that the angular dependencies of the phase distortions on the meridional angle weakly change for different materials. The only exception is osmium for which the phase deformation was extremely low. Optical constants of materials used in these calculations were taken from (Palik, 1985).

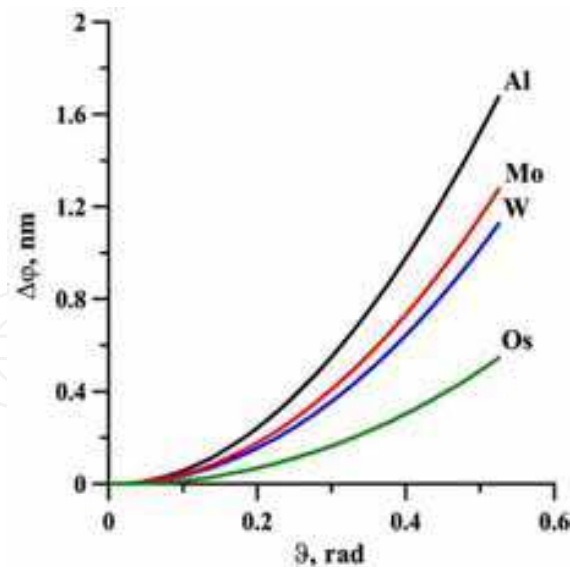


Fig. 10. Angular dependencies of the phase distortions on the meridional angle for different materials.

By this means a fundamental limitation of the point diffraction interferometer measurement accuracy is caused by the aberrations of the reference spherical wave induced by the interaction and propagation of secondary waves through the screen material. These aberrations are liable to reach a few nanometers depending on the angular aperture. If we take into account the polarization characteristics of the light, the aberration of the reference wave increases a few times depending on azimuth angle (Dorofeev, 2009).

The quality of a diffracted wave strongly depends on wave aberrations of preliminary optics focusing the laser beam and the accuracy of adjusting the laser beam axis in respect to the pin-hole center (Otaki et al., 2002). All these limit the working aperture of the interferometer and result in the necessity of testing high-aperture optics zones. The following stitching procedure of the zonal data raises additional errors. All of these disadvantages hinder to widespread use of the point diffraction interferometers in an industry. Taking into account all of these problems and limitations the problem of searching for alternative and more perfect methods for the spherical wave generation becomes very urgent.

5. Spherical wave source on the basis of tipped fiber

The sources of the spherical wave based on tipped down to a sub-wave exit aperture of the single mode fibers are free from the many of mentioned above problems. The application of such fibers as a reference spherical wave source for the point diffraction interferometers has been proposed in (Klimov et al., 2008). In Ref. (Chkhalo et al., 2008) the aberrations of the wave generated by the sources at the wavelength of He-Ne laser $\lambda=633$ nm have been studied. These investigations have demonstrated a number of advantages of spherical wave sources as compared with the conventional ones based on a pin-hole in an opaque screen. One of the advantages is connected with the fact, that in the optical fiber the eigenmodes are excited and correspondingly the quality of the diffracted wave does not depend on aberrations and the mechanical adjustment of the preliminary optics.

A high degree of homogeneity of the diffracted wave ($\lambda/d > 1$) is combined with a high intensity because the light is input into the fiber using high-efficiency methods through a 5-

μm -diameter core. The convex shape of the source, Fig. 11, decreases the “tip” effect bound to the interaction of the off-axis rays with a metallized part of the fiber along the perimeter of the exit aperture. The lack of a flat screen around the source significantly decreases diffracted wave distortions connected with the light polarization. The well developed methods for handling optical fibers make it possible to easily control the polarization parameters of the diffracted radiation and implement various schemes for interference measurements. For instance, two or even more coherent sources can be organized with the given polarization of each other.



Fig. 11. Photographs of the fiber based source taken with scanning electron microscope (marked as a) and b)) and the source with on optical connector.

The quality of the diffracted wave of the tipped fiber based source was studied with an interferometer (Kluenkov et al., 2008) at two wavelengths: $\lambda=633\text{ nm}$ (He-Ne laser) and $\lambda=530\text{ nm}$ (second harmonic of Nd-YAG laser). As opposed to the former experiments when in the measurement scheme an optical observation system collected the interfering fronts onto the CCD-camera, in present work the data obtained by the direct detection of the fronts on the window-free CCD-camera are given. As the experiments showed both the observation systems and even a thin glass window introduce a significant, at the level of parts of nanometer, error into the measurements.

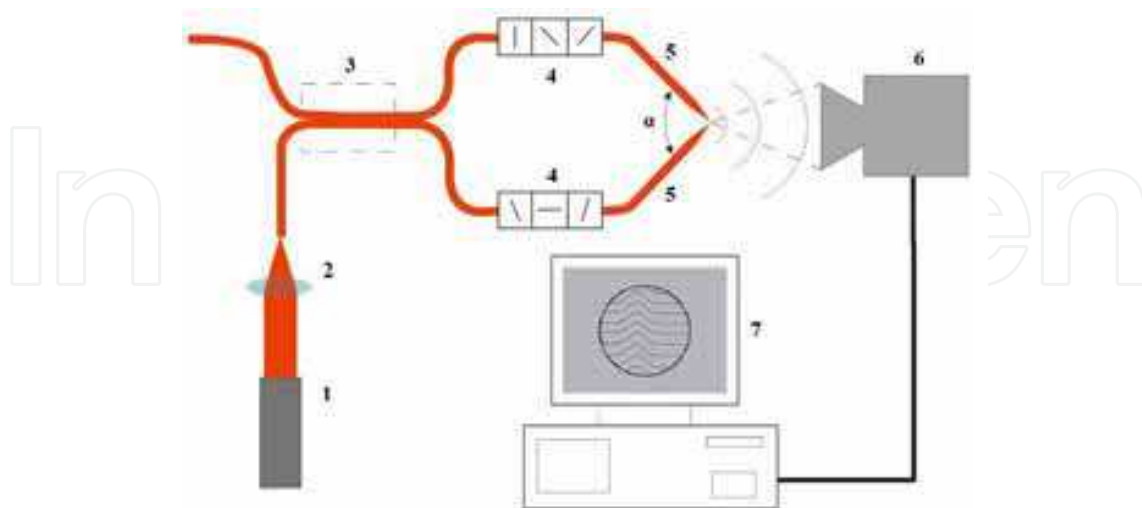


Fig. 12. Experimental setup for studying the wave front deformations of the tipped fiber based sources of spherical wave. 1 is a laser, 2 is a system for input the light into the fiber, 3 is a single mode fiber optics coupler, 4 is a polarization controller, 5 are sources under study, 6 is a CCD-camera and 7 is a computer.

The new experimental setup is given in Fig. 12. Polarization controllers (item 4 in Fig. 12) allow to transform an elliptical polarization of the light at the output of the sources into a linear one as well as to superpose the polarization planes, which provide the best contrast of the interference pattern. The distance between the sources determining the fringe number (a wedge between two interfering wave fronts) was varied in the range of 1-10 μm . The measurements were carried out for different angles α between the source axes. The numerical aperture was varied by approaching (moving off) the CCD camera in respect to the sources. A typical interferogram and a wave aberration map obtained in the experiments are shown in Fig. 13. The operating wavelength was $\lambda=530\text{ nm}$.

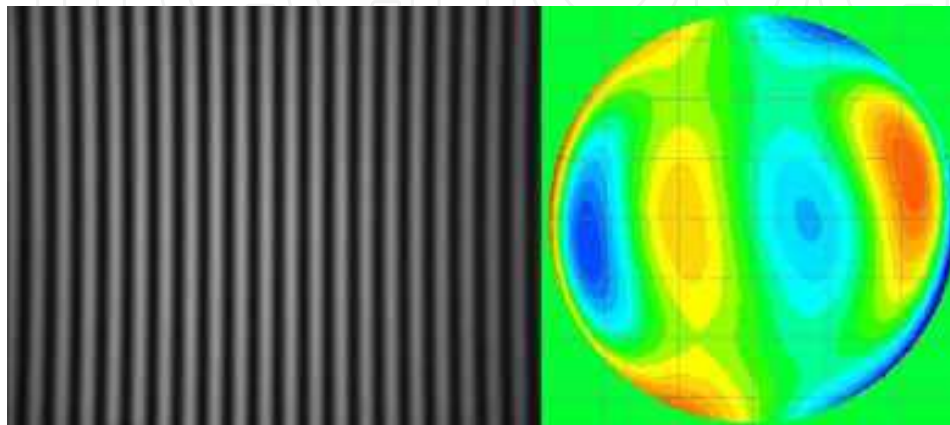


Fig. 13. A typical interferogram and a wave aberration map observed in the experiments obtained at a wavelength $\lambda=530\text{ nm}$.

The measured dependencies of the wave deformation *RMS* on numerical aperture *NA* of this couple of sources are given in Fig. 14. The pictures correspond to the measurements in small (left) and in large (right) numerical apertures. Left graphs on both pictures correspond to the experimental data. The data obtained with the interferometer installed on the synchrotron ALS in Berkeley, USA, are marked by stars. The interferometer using a pin-hole in an opaque screen as a reference spherical wave source, operates at the wavelength $\lambda=13.5\text{ nm}$ and is considered as a reference for the measurement accuracy among the point diffraction interferometers (Naulleau et al., 1999). It is clearly seen from the pictures that wave front aberrations of the source, developed in this work, are even less as compared with the ALS-sources despite a longer operating wavelength.

When analyzing the obtained experimental data there is a need to pay attention to two facts:

- Relatively “high”, of order $\lambda/1000$, total aberration of the diffracted waves is observed at large numerical apertures ($NA\approx 0.3$);
- Regular structure (symmetry) of the wave front deformation map is clearly seen.

Such maps and statistical values of the deformations are practically found for all couples of so called “high quality” sources. The wedge direction between interfering fronts (a line passing through the sources) represents itself as the axis of the symmetry. Particularly, the deformation map can be put “horizontally” by turning the wedge through 90 degrees. All of this points to the presence of an aberration, caused by some kind of physical reason rather than by technological fluctuations. This aberration rises with the increase of the observation angle just as it is shown in Figs. 9 and 10. In case of understanding the physical nature of this aberration it can be taken into account when reconstructing the true wave deformation (surface shape) that results in increasing the working aperture of the interferometer by a few times.

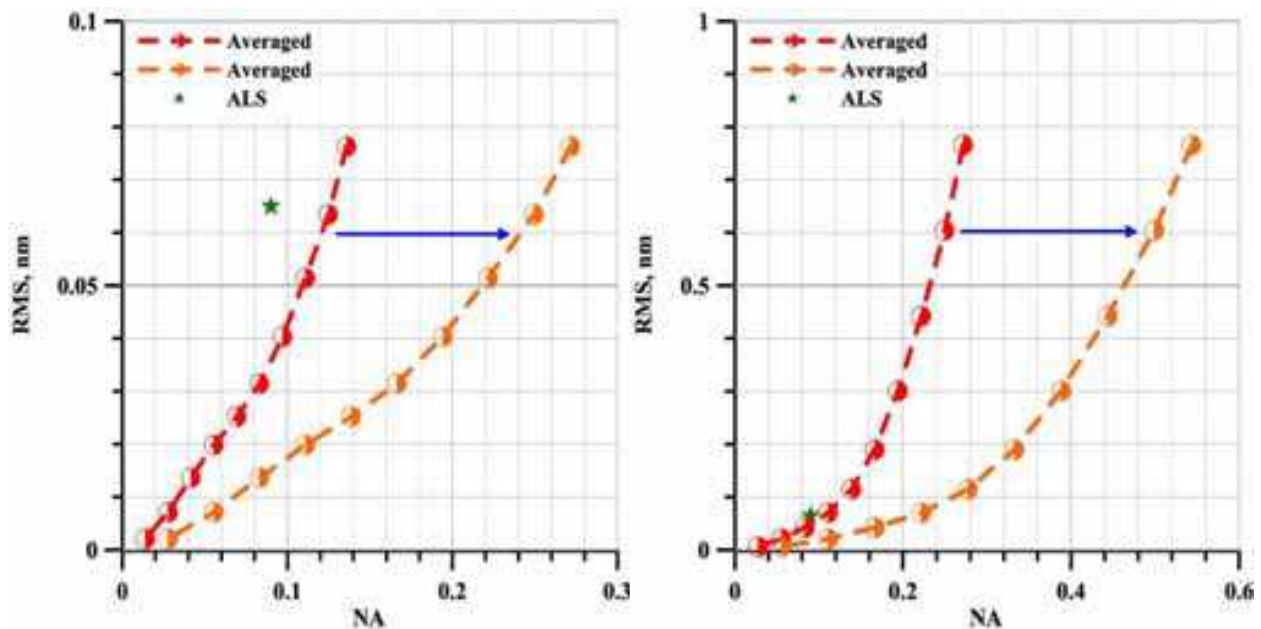


Fig. 14. Averaged over 9 measurements total wave front deformations of couple of the fiber based spherical wave sources depending on numerical aperture (left graphs in both pictures) and ALS-data (Naulleau et al., 1999) (stars). Working wavelength is $\lambda=530$ nm. First picture corresponds to lower and right – to the higher numerical apertures. The right graphs in the pictures are corrected according to the geometry of the experiment.

This fact of the uniform angular dependence of the aberration let us interpret in a new manner the measurement data obtained in ALS and in our experiments. In the Young's experiment carried out in ALS the least distorted parts of the diffracted waves round their own axes interfere. Correspondingly *RMS* of the aberration is calculated over the range of the cone, limited by the numerical aperture *NA*. Opposite to that in our case side parts of the wave fronts interfere, Fig. 12, in the range from zero degree up to a double value of the angular aperture of the wave front. In other words, in the search for the wave front aberration *RMS* the averaging is performed over a double numerical aperture, $2NA$. Therefore, the measured dependences presented in Fig. 14 (left graphs) can be corrected in the manner as it is shown by arrows (right graphs). As it is seen from the picture the source of the reference spherical wave based on a tipped single mode fiber has a substantially lower wave front aberration and a higher working aperture as compared with the conventional one based on pin-hole in an opaque screen.

6. Diffraction interferometer based on a single mode fiber with the sub-wave exit aperture

On the basis of a tipped fiber source of the reference spherical wave the laboratory sample of an interferometer has been developed and manufactured, which optical scheme and photo are presented in Figs. 15 and 16. The interferometer is installed in a basement thermostated room on a bearer separated from the house footing. For the additional protection against vibrations, the instrument is installed on 12 bellows under 1.6 bar pressure. Since the measurement accuracy is extremely high, the turbulent air flowing inside the interferometer and effecting optical paths along the rays, can introduce additional errors. To solve these problems, the interferometer is placed into a vacuum chamber which is pumped out down to a pressure of 1 Pa.

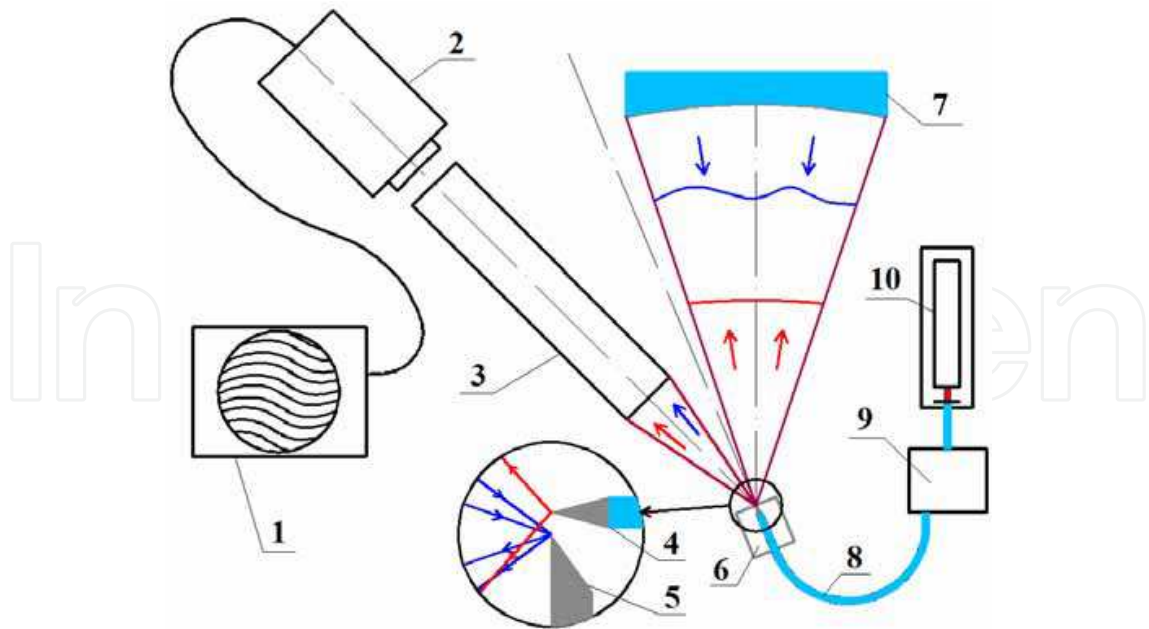


Fig. 15. Optical scheme of the interferometer:
 1 - PC, 2 - registering system, 3 - observing system, 4 - source of spherical wave, 5 - flat sharp-edge mirror, 6 - three-axes-controlled precision bench, 7 - tested concave surface, 8 - single mode optical fiber, 9 - polarization controller, 10 - laser.



Fig. 16. Photograph of the vertical vacuum interferometer.

The optical scheme shown in Fig. 15 corresponds to the interferometer for studying concave spherical or weakly aspherical surfaces. The spherical wave source (item 4, Fig. 15) is mounted on a high-precision three-axis-controlled bench (item 6, Fig. 15) in the direct, in a distance of several micrometers, proximity from the flat mirror (item 5, Fig. 15). The reference spherical wave, which after reflecting from the studied surface (item 7, Fig. 15) carries the information about its form, is focused on a flat mirror and being reflected from it goes into the CCD registering system, where it interferes with a part of the reference front directly propagating to the detector.

The main disadvantage of this scheme is connected with the fact that the investigated sample is irradiated by the most distorted side part of the wave front that practically halves the interferometer operating numerical aperture. For solution of this problem in (Kluenkov et al., 2008) the scheme of the interferometer with two low-coherent sources of the reference spherical waves has been proposed (Fig. 17). In this scheme one source forms the spherical wave, «Spherical wave №1», irradiating the investigated surface, while the spherical wave of the second source, «Spherical wave №2», is directed into the registering system. The radiation reflected from the investigated surface contains the information on its shape and after reflecting from the flat mirror is directed to the registering system, where interferes with the reference «Spherical wave №2». The main advantage of the scheme is that the axes of the wave fronts coincide with the axes of the investigated surface and the registering system which provides the minimal deformations of reference fronts.

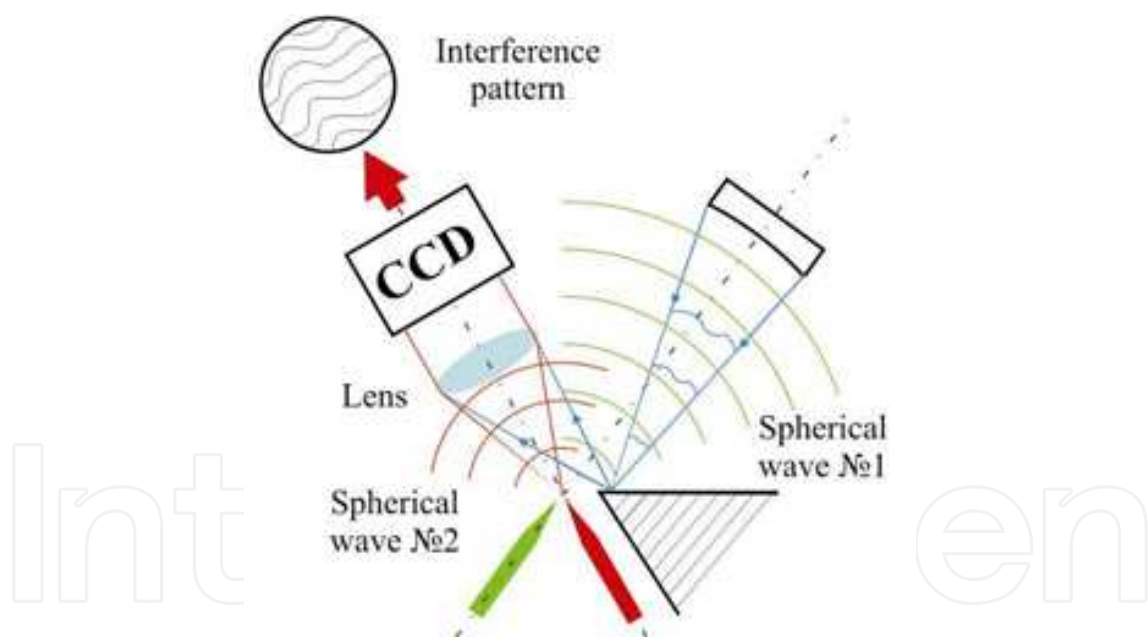


Fig. 17. Scheme of the low-coherence diffraction interferometer with two sources of the reference spherical wave.

As a source of the radiation a super-luminescent diode with a coherence length about 20 microns is applied. It prevents parasitic interferences of wave fronts produced by different elements of the optical scheme. For observing the "correct" interference the optical path of the light of source №2 is increased by a double distance from the investigated surface to the sources. In this case the interference is observed only for the noted above wave fronts. The radiation of the source №1, directly going into the registering system, creates only a background signal on the detector.

As it was already marked, in diffraction interferometers a divergent spherical wave is used as a reference wave. It imposes a number of restrictions on the interferometer capabilities. Strictly speaking, with their help it is possible to investigate only concave spherical and slightly aspherical surfaces and objectives. The measurement of the form of strongly aspherical concave or even spherical, but convex, surfaces demands using additional optical elements, transforming the reference divergent spherical wave to a new one which front is close to the surface shape under study.

Of special interest are interferometric measurements of objective wave front deformations, for example, for final certification of the objective wave aberrations, or for objective adjustment directly in an interferometer, or in the case of the objective application for studying convex spherical surfaces. In Fig. 18 the scheme and photograph of measurements of six-lens objective in the interferometer are shown. In this scheme two coherent sources are used. The measured data of the wave deformation were: $PV = 42.3 \text{ nm}$ and $RMS = 8.2 \text{ nm}$.

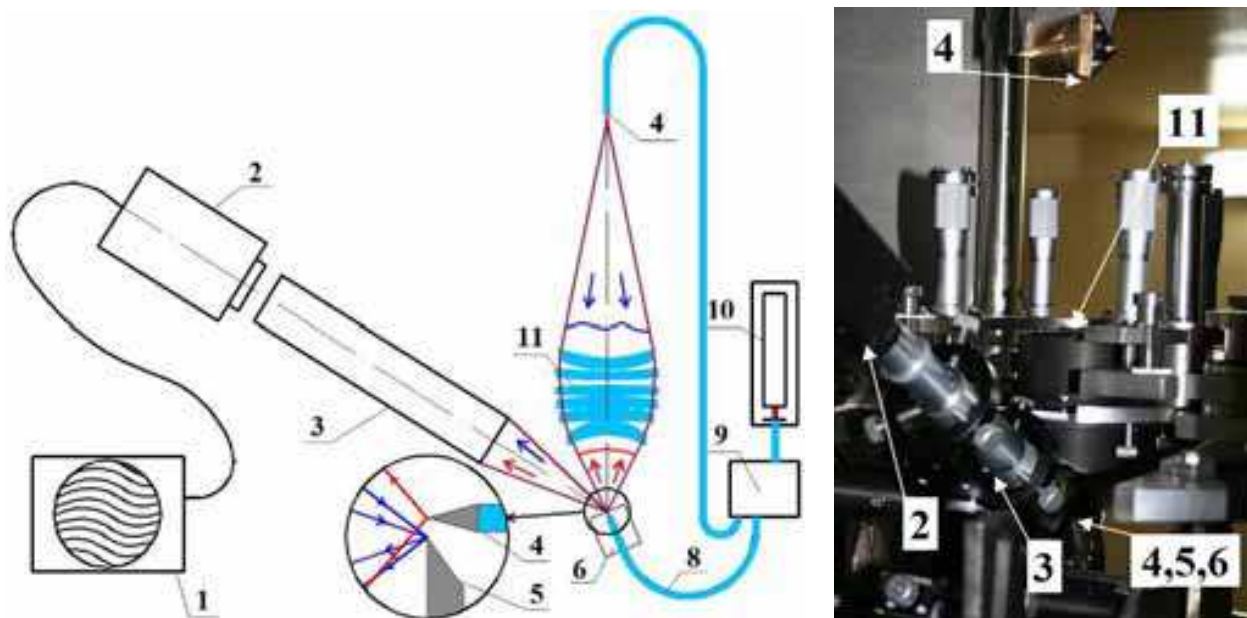


Fig. 18. Scheme of the interferometer with two coherent sources of the reference spherical wave (left) and photograph in the interferometer (right) for testing six-lens objective. 1 – PC, 2 – registering system, 3 – observing system, 4 – source of spherical wave, 5 – flat sharp-edge mirror, 6 – three-axes-controlled precision bench, 8 – single mode optical fiber, 9 – polarization controller, 10 – laser, 11 – studied objective.

The certified objective was used for the interferometric measurement (Fig. 19) of a convex spherical surface of a special compensator which in turn later on was applied for studying the concave aspherical surface for a double-mirror objective. For reconstructing the true shape of the convex surface the expansion coefficients at basis polynomials corresponding to the objective aberrations were deducted from the measured ones.

Aspherical surfaces are used in the majority of high-resolution optical objectives in order to widen the field of view of the optical systems. Direct testing of aspherical surfaces by using an interferometer with the spherical reference wave is often difficult or even impossible. For example, Fig. 20 a) shows the interferogram for a concave aspherical substrate with about $7\text{-}\mu\text{m}$ deviation of the surface from the nearest sphere. The measurements were carried out by using the basic scheme shown in Fig. 15. It is evident, that a large number of fringes makes

the position determination of the minima almost impossible. Moreover, the upper part of the interferogram is simply not there, which is explained by a large, about 100 μm , diameter of the focusing spot for which the beam partially propagates above the edge of mirror (item 5, Fig. 15) and misses the measurement system.

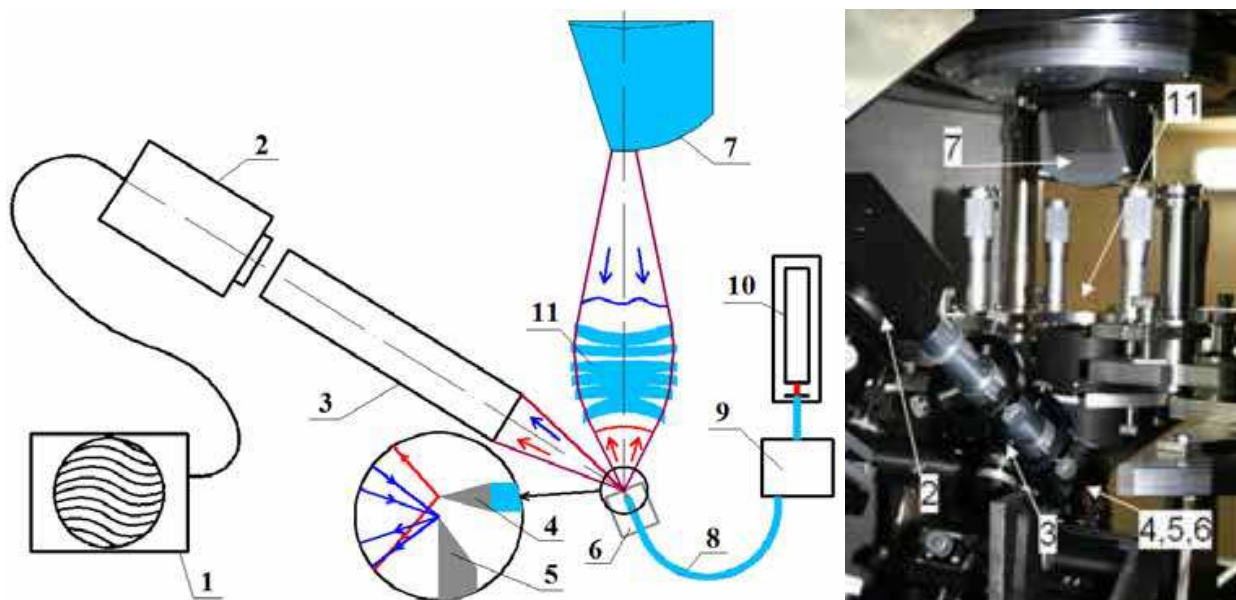


Fig. 19. Optical scheme (left) and photograph of units (right) in the interferometer for certification of convex surfaces. Designations on the scheme are the same, as in Fig. 15.

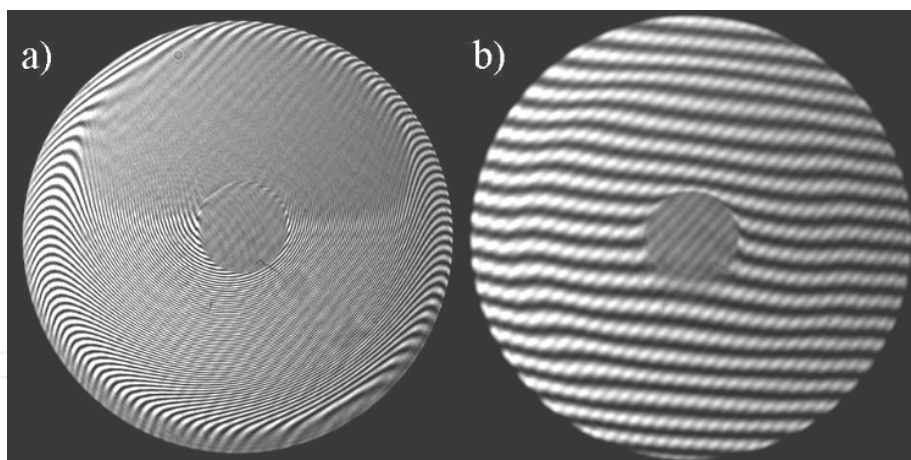


Fig. 20. Interferograms from the aspherical concave mirror M2 obtained without wave-front corrector (a) and using corrector (b).

One of the most effective solution of this problem is the use of wave-front correctors, i.e., special optical elements that transform a reference spherical wave front into an aspherical one which shape is identical to the shape of the studied surface. In order to take into account the wave-front distortions due to errors of the corrector itself, its surfaces should be only spherical. In this case, it is possible to test these surfaces with subnanometer accuracy by using a spherical reference wave interferometer by the techniques stated above.

The scheme for testing the concave aspherical surface by using a corrector is presented in Fig. 21. The parameters of the corrector suitable for testing the concave aspherical surface,

i.e. radii of the surfaces, thickness, and the distance from the reference wave source to the top of the first surface, were calculated by minimizing the difference of longitudinal aberrations of the tested aspherical surface and the corrector, described in (Malacara, 1992; Puryaev, 1976) in detail. The calculated root-mean-square deviation of the wave front after the corrector from the investigated aspherical shape was $RMS=\lambda/1810$. This suffices for testing the mirror surface of a nanolithographer with a double-mirror objective. It is clearly seen from Fig. 20 b), that the interferogram from the aspherical surface, obtained by using such a corrector can be reliably processed.

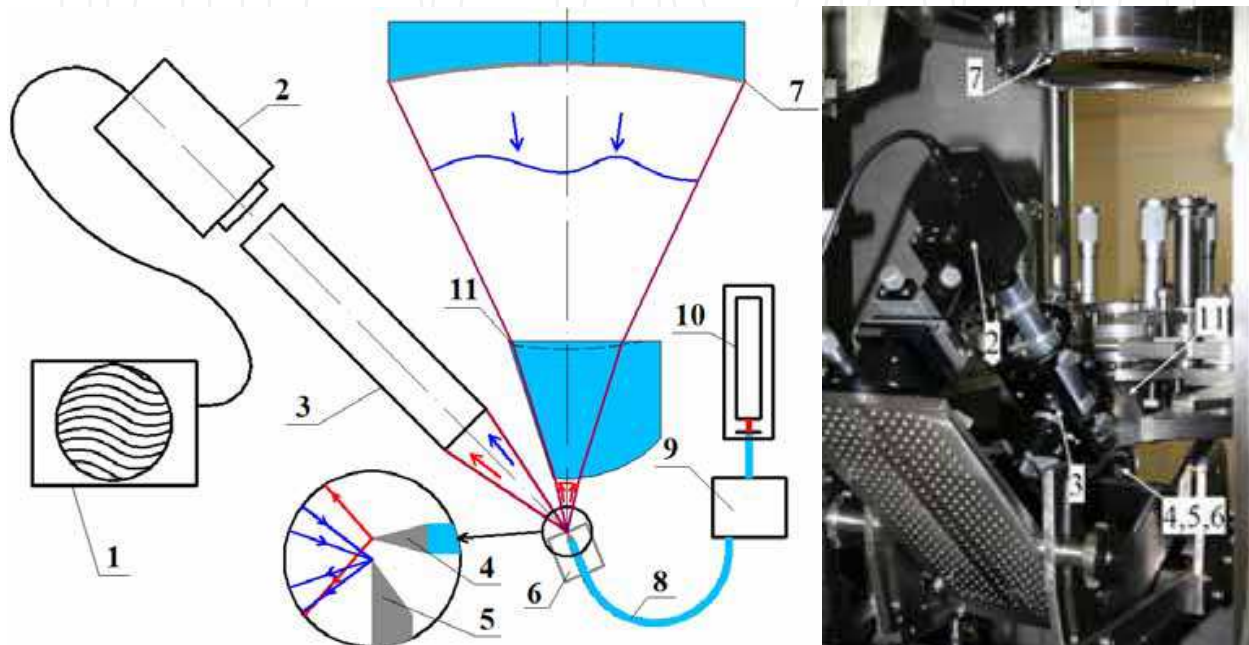


Fig. 21. Optical scheme (left) and photograph of units in interferometer (right) for certification of concave aspherical surfaces using corrector. 1 - computer, 2 - registering system, 3 - observation system, 4 - spherical wave source, 5 - flat mirror, 6 - 3D precision table, 7 - investigated concave aspherical surface, 8 - optical fiber, 9 - polarization controller, 10 - laser, 11 - corrector.

The analysis of the influence of misalignment in the measurement optical scheme and a thickness error of the compensator on "asphericity" of the wave-front passing through the corrector and, accordingly, on the measurement accuracy has shown, that the requirements for these characteristics of the optical scheme are easily performed in practice. In particular, the error of a compensator thickness within the limits of ± 0.1 mm leads to a wave front aberration at the level of $\lambda/1000$.

Studying of the convex aspherical surfaces is complicated by the fact that besides the corresponding transformation of a spherical front into an aspherical one, the corrector must provide a converging front of the wave. All of these essentially complicate both the calculation, and the design of the corrector. In particular, in some cases it is necessary to use aspherical surfaces, or more than one lens. In the case of optics for Schwarzschild objectives this problem is solved easily enough. As a corrector the mating concave aspherical mirror, which surface has been preliminary tested by using the corrector system described above and corrected according to the procedure described in the next section, can be used. The measurement scheme is presented in Fig. 22. This scheme can be applied for the final

adjustment and certifications of the objective. It is noteworthy to mention, that this method can be applied for a convex spherical surface characterization too besides using additional objectives, as it is shown in Fig. 19.

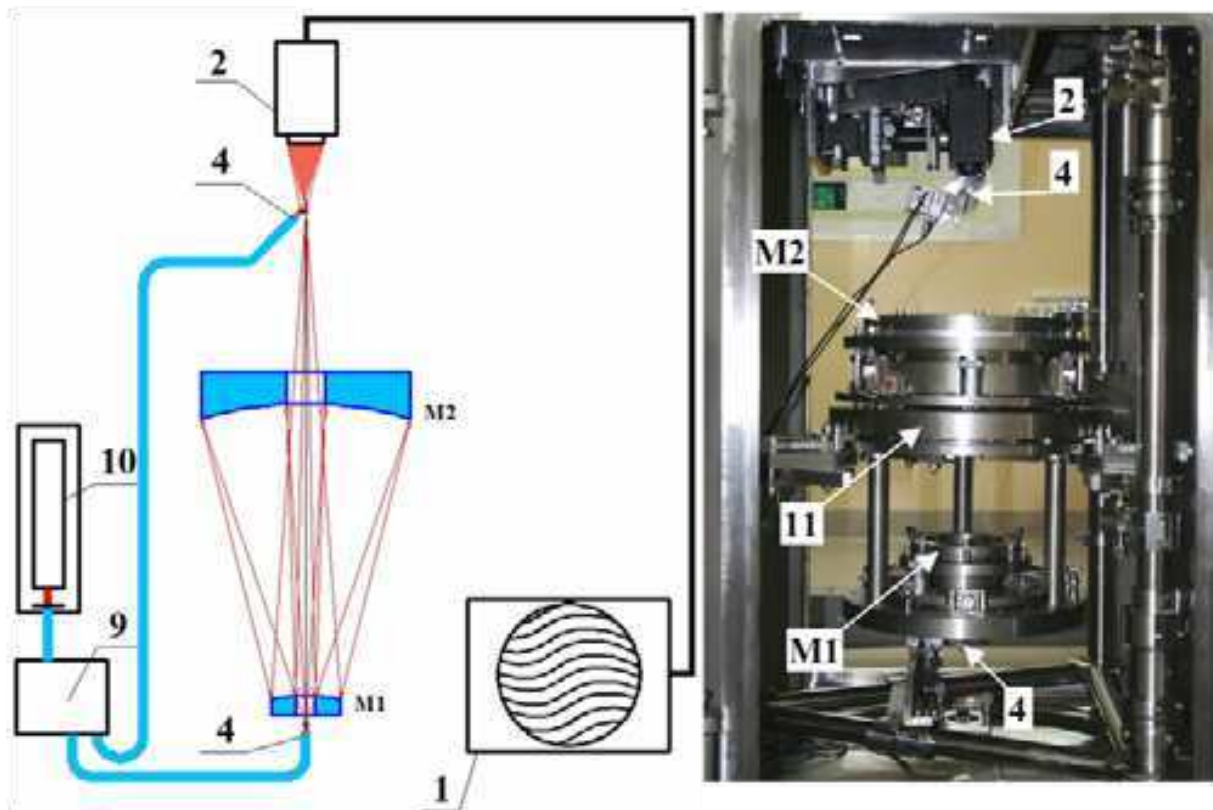


Fig. 22. Measurement scheme of aspherical convex mirror M1 using mirror M2 as a wave-front corrector. 1 - computer, 2 - CCD camera, 4 - spherical wave source, 9-polarization controller, 10 - laser, 11 - Schwarzschild objective, M1 and M2 - convex and concave aspherical mirrors.

The measurement accuracy provided by the interferometer depends on many factors, including the quality of the reference-wave source, the accuracy of determining the positions and a number of interference minima, and the accuracy of mathematical retrieval of the surface (wave-front) shape using a limited number of experimental points, and the number and degree of the polynomials. In turn, the accuracy of determining the minimum positions is strongly dependent on the width of the interference pattern, the degree of pollution of the interference pattern by "parasitic" interference, the method of its rejection, the uniformity and intensity of the interfering fronts, and a number of other unmanageable factors.

In this work, the interferometer measurement precision was evaluated by studying the rotations of the measured surface maps corresponding to the physical turn of the tested detail. The idea of this method is the following. If the interferometer provides zero-error measurements then when the detail is rotated the measured surface map should turn correspondingly and the measured statistical parameters of the surface shape deformations should remain unchanged. The measured surface deformation maps of a spherical substrate with a numerical aperture $NA=0.14$ corresponding to different rotations of the detail are

presented in Fig. 23. The figures demonstrate that the turn of the maps is well observed, and the statistical parameters of the deformations change within the limits of $RMS=3.07\pm 0.055$ nm. This test confirms the high measurement accuracy provided by the interferometer, which is sufficient for many lithographic applications.

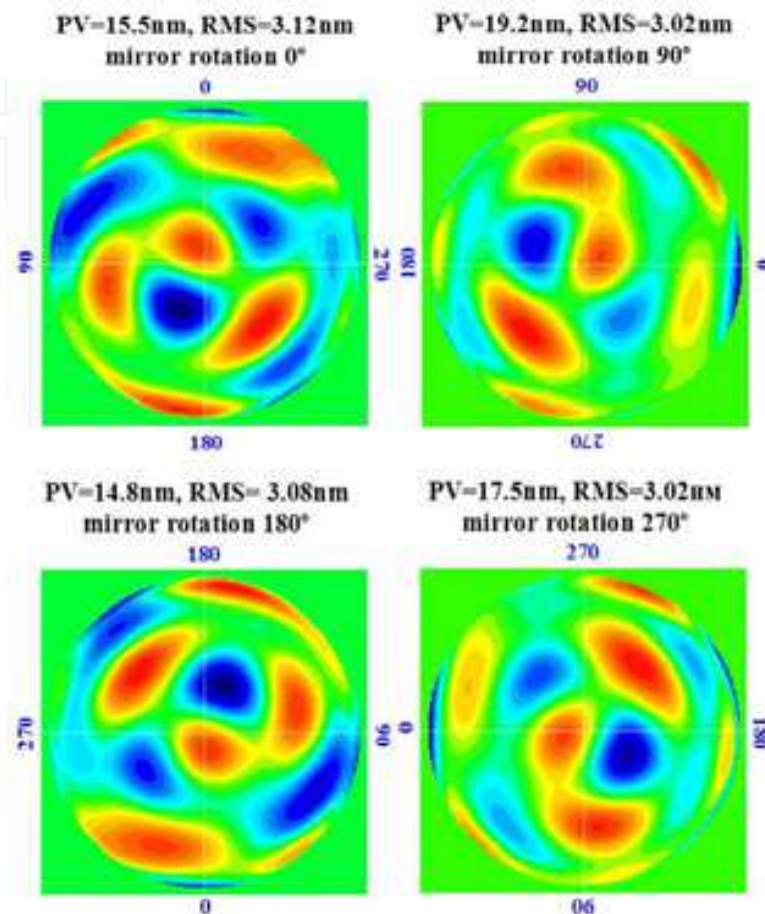


Fig. 23. Maps and statistical parameters of the surface form deformation corresponding to rotations of the spherical mirror by 0, 90, 180 and 270 degrees.

To summarize this section it is possible to ascertain, that the developed interferometer with the diffraction reference wave provides a precision certification of the high-aperture optical surfaces and systems to the subnanometer accuracy.

7. Shape correction of optical surfaces to subnanometer accuracy

The developed precise techniques for measuring the shape of optical surfaces made it possible to pass to the main stage: the correction of the surface shape made with traditional accuracy, $\lambda/2 - \lambda/20$, depending on the type of optics, up to $\lambda/1000 - \lambda/2000$. In the context of the given work two methods of correction have been developed: a vacuum deposition of thin film coatings and ion etching of previously deposited films through metal masks. An extremely high accuracy of correcting the surface shape imposes specific requirements on the correction method.

1. As a result of the correction process the microroughness of the corrected surface (as a rule, it is initially supersmooth) should remain at the initial level.

2. In the case of a shape correction by means of a local thin film deposition the correcting layers should not distort the substrate surface shape due to intrinsic stress, i.e. they should have a minimally possible stress.
3. The correction method should provide the deposition or the removal of materials in a wide range of thickness (1-300 nm) with the accuracy not worse than several percents. This problem is especially urgent in the last correction stages, when the thickness of the layers to be deposited (removed) is about one nanometer.
4. The film materials should allow their complete removal from the substrate (for example, chemically) without changing the initial surface shape and microroughness. It allows repeating the correction process in the case when the previous correction attempt failed.

Researches on stress compensation in multilayer structures and on a substrate restoration have shown that a material meeting all these requirements is *Cr/Sc* multilayer structure (Salashchenko, 2001). The deposition of coatings was made by the magnetron sputtering method. The scheme of the correction process and the photograph of the installation are shown in Fig. 24. Vacuum in the chamber was $(0.7-1) \cdot 10^{-6}$ Tor, pressure of working gas (argon) was $(0.7-0.9) \cdot 10^{-4}$ Tor. The characteristic power on DC magnetrons was 300-400 W. The film thickness control of the deposited layers is performed by varying the passage speed of the corrected surface above the magnetrons sources. The stabilization of the discharge power and the argon pressure were provided at the level of 0.1 %. The predetermined distribution of the layer thickness over the substrate surface was reached due to the application of figured diaphragms mounted between the magnetron sources and the substrate. In addition the substrate rotates around its axis. Local values of the film thicknesses over the substrates were measured with an x-ray reflectometer at 4.47 nm wavelength. The details of these measurements will be shown below.



Fig. 24. Photograph of a technological facility and scheme of surface shape correction by means of multilayer film deposition through masks.

The operational experience with this technology has shown a number of important advantages. Firstly, the roughness of the film surface practically does not depend on the angle of incidence of the atoms in respect to the substrate that allows to carry out the

correction procedure at normal angles. It reduces shadows on the surface, increasing the localness of the correction, correspondingly. Secondly, the high accuracy of the layer thickness control, up to 1 %, provides a high reproducibility of the process. The film-correction method proved to be efficient for initial stages, in which the layers with of tens-hundreds nanometers are deposited in a single correction. The process becomes unstable as the thickness of deposited layers decreases down to the units of nanometers. Correcting films have changed the proper color that is connected with films oxidation at initial stages of deposition. The distribution of oxygen in depth of scandium film obtained with the help of a secondary ion mass-spectroscopy (Drozdov et al., 2009) is given in Fig. 25. The figure shows an increased content of oxygen on the film surface and at the film-substrate interface. Other serious disadvantages of the thin-film-correction method has a discrete and iterative character of the process. After each iteration it is necessary to vent the vacuum chamber, to make a new diaphragm, to pump the chamber again. All this strongly decreases the throughput of the process.

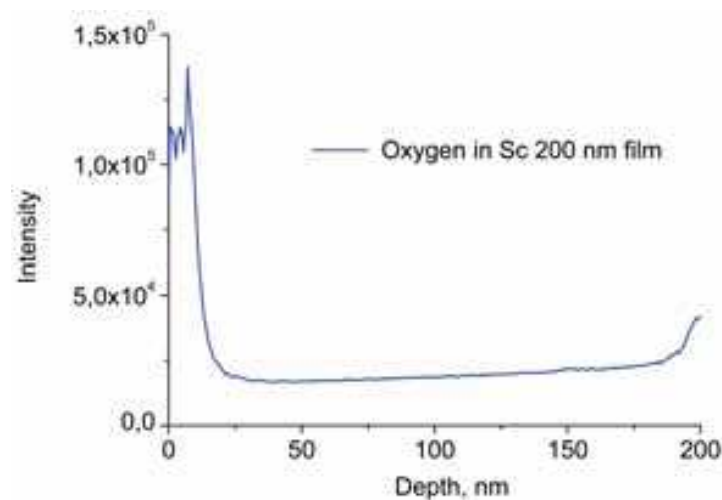


Fig. 25. The distribution of oxygen in depth of scandium film deposited onto Si-substrate.

Therefore the application of ion-beam etching at the final correction stage looks very attractive. This method allows, in particular, when focused ion-beams are used, to realize the "maskless" correction without frequent opening of the installation to atmosphere. Now this method is widely used for substrate form correcting and even for final ion-beam polishing in optical industry (Allen et al., 1991; Chason & Mayer, 1993; Ghigo et al, 2007). Recently an intensive literature has evolved which is devoted to the application of this method for the precision correction of substrates for projection EUV lithography (Dinger et al., 2000; Murakami, 2007).

For the ion beams, applied for the surface shape correction of substrates for EUV and soft X-ray optical elements, a number of requirements are imposed, the basic of which is the preservation of the surface roughness at an initial (supersmooth) level even when the removed layer depth reaches a few hundreds of nanometers. Therefore an optimization of ion energy and incidence angles of the ions on the corrected surface at different depths of material removal is an actual problem.

Other problems inviting a further investigation are connected with some features of the ion-beam etching at an extremely small depth (≈ 1 nm) removal of materials.

The experiments have been performed on the installation (Fig. 26) with the "Cauphman» type ion-beam source KLAN-103M (Website Platlar Company, 2009). The basic advantage of

this source is the possibility of working with small ion energies, $E_i = 50- 300$ eV, at a significant current density.



Fig. 26. Photographs of installation for substrates surface shape correction by ion-beam etching.

The main characteristics of the ion source are: the operating gas is argon or other inert gases; the maximal diameter of the ion beam is 100 mm; the maximal ion current is 100 mA; the maximal ion current density is up to 2.3 mA/cm²; the range of ion energy regulation is 50-1500 eV at the energy spread of ± 3 eV; the discharge working voltage is 35-50 V; the thermo-cathode is made of thoriated tungsten (0.3 mm in diameter) filament. Presence of charge-neutralizer (additional thermo-cathode) allows compensating the ion beam charge that provides using the ion source for correction substrates of dielectric materials too.

The measured dependence of the etching rate of Cr/Sc coating on the removal depth taken at ion energy $E_i=200$ eV and grazing incidence angle of $\theta = 42^\circ$ is shown in Fig. 27 by dots. It is evident that at the initial stage of the etching, the removal is less than 120 nm, practically a linear increase of the etching rate from the removal depth is observed. At a very small etching depth, $h < 10$ nm, a wide scatter of the etching rate values is observed. Considering the data of the secondary ion mass-spectrometry, Fig. 28, such a behavior of the etching rate can be explained by oxidation of the sample surface. The etching rate of the oxide layer is significantly lower as compared with pure Cr/Sc material. If take this into account the calculated etching rate, a solid line in Fig. 27, matches well the experimental data. The observed instability of the etching rate at $h < 10$ nm might be explained by the variation of the oxidized layer depth in various samples. When samples were etched by a neutralized beam (stars in Fig. 27), no changes of the rate were observed. With the increased ion energy up to 300 eV, Fig. 29, such instability of the etching rate is not observed either. According to atomic-force microscopy measurements the surface roughness remained constant, at the level of 0.2 nm, down to 400 nm removal depths. For the ion energy of $E_i=300$ eV when the etching depth exceeds 80 nm an increase of surface roughness is observed (Fig. 30).

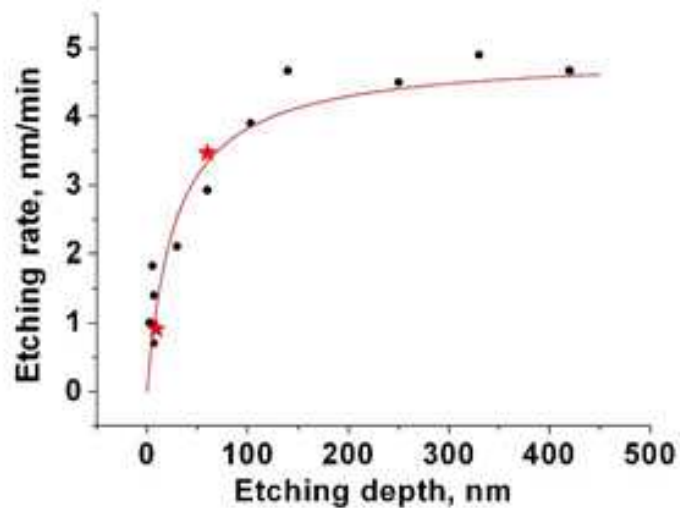


Fig. 27. Dependence of etching rate on removal depth of *Cr/Sc* multilayer structures: dots are experiment with ions, stars are experiment with neutrals and line is calculation accounting etching of the oxidized layer. Ion energy $E_i = 200$ eV and current $I_i = 60$ mA.

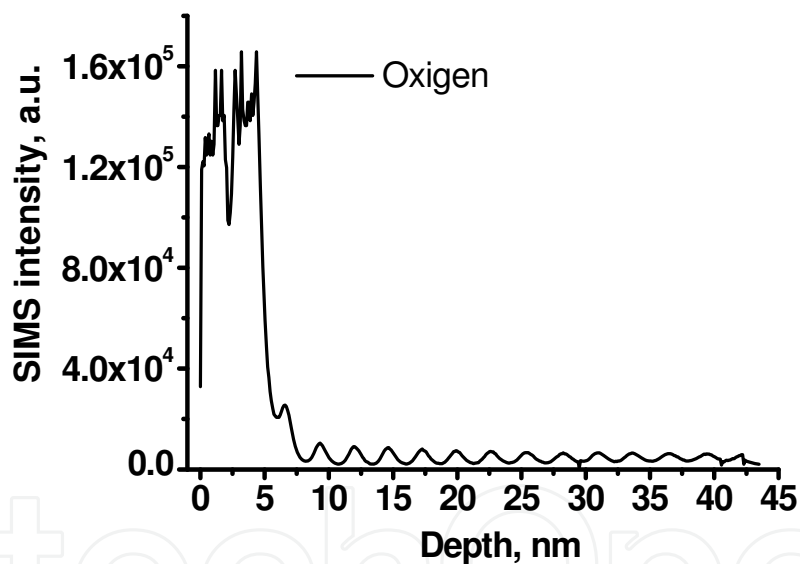


Fig. 28. Typical distribution of oxygen atoms on depth of *Cr/Sc* multilayer structure taken by secondary ion mass-spectrometry.

The dependences of etching depth on an ion dose (the dose is the product of ion current and etching time) both from the ion current at fixed time, and from the time at fixed current, show a good linearity, that is useful from the practical point of view because it allows to easily define the necessary etching time at a given ion current. The example of the dependences of the etching depth on the dose is given in Fig. 31. The dashed line corresponds to the linear approximation of the dependence and line with squares represents the experimental data. It should be noted, that the experiments carried out with greater ion energies, up to $E_i = 1.5$ keV, have shown a fast growth of the surface roughness, even at small, nearby 20° , grazing angles of incidence of the ions on the surfaces (Chkhalo et al., 2008).

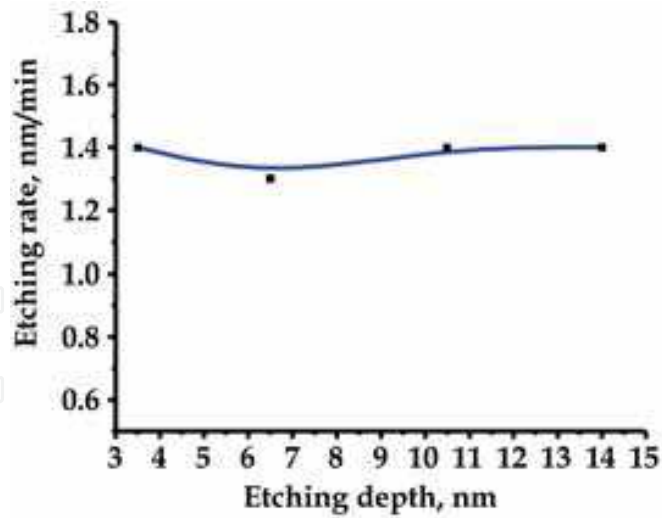


Fig. 29. Dependence of ion etching rate on etching depth of Cr/Sc multilayer structures at ion energy $E_i = 300$ eV (area of small removal depths).

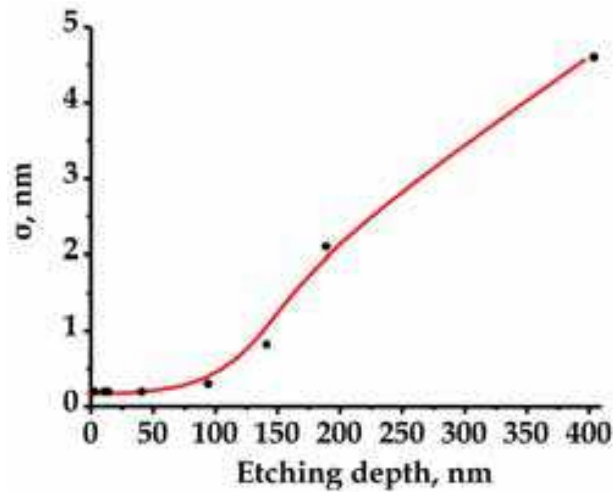


Fig. 30. Dependence of surface roughness of Cr/Sc multilayer structures on etching depth at sputtering by argon ions with energy $E_i = 300$ eV.

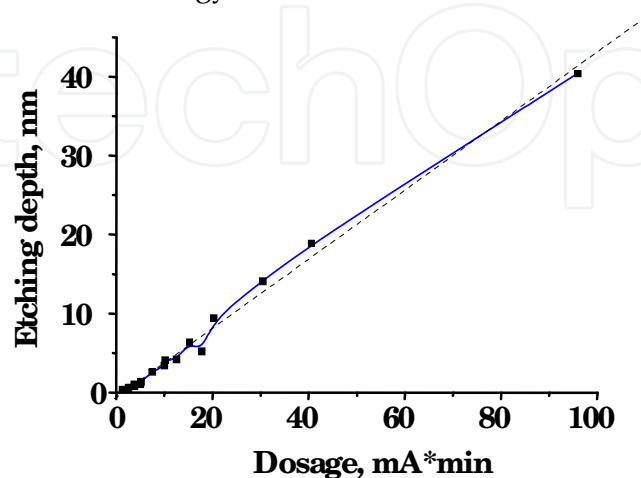


Fig. 31. Dependence of etching depth of the Cr/Sc multilayer structures on ions doze, at ion energy $E_i = 300$ eV. - - - linear approximation of the dependence.

For correcting the surface shape of substrates for imaging X-ray optics when the subnanometer form accuracy is required, the following strategy providing minimal time expenses has been chosen. At the initial stage when peak-to-valley values ($P-V$) of the surface shape are 50-200 nm, the local deposition of the thin films is applied. Then, at the reduction of the $P-V$ values down to 10-20 nm the ion beams with the energy of 200 eV are used. At the final correction stage the 300 eV-ions are applied. Figure 32 illustrates the result of using this correction procedure for a spherical substrate with a numerical aperture of $NA=0.25$ (the diameter is 130 mm and the curvature radius is 260 mm), which was initially the standard etalon for a conventional interferometer. The initial surface map is shown in Fig. 32 a). The parameters of the surface were $P-V=42.6$ nm and $RMS=7.3$ nm. The surface shape improved to $P-V=7.3$ nm and $RMS=0.6$ nm (Fig. 32 b)). Thus, a root-mean-square deviation of the initial surface shape from an ideal sphere has decreased in 12 times, i.e. in units of the interferometer working wavelength ($\lambda=0.633$ μm) it has become better than $\lambda/1000$. The photograph of this mirror mounted on a metal frame is given in Fig. 33.

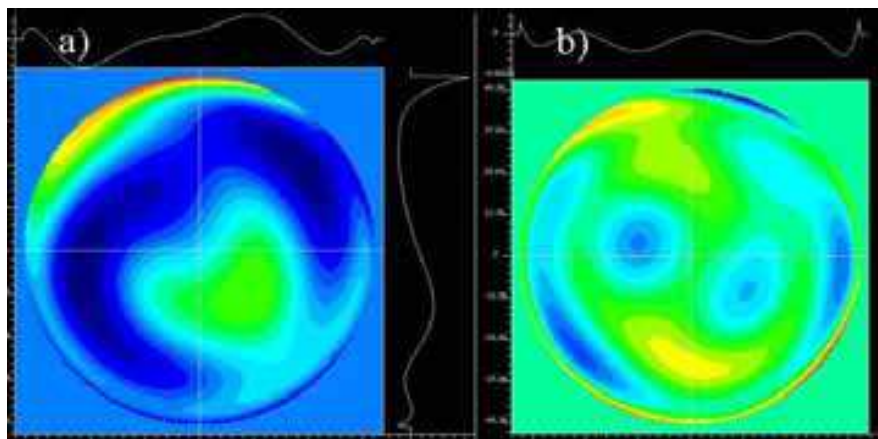


Fig. 32. Maps of deviations of the spherical surface shape from the nearest ideal sphere: a) initial shape ($P-V=42.6$ nm, $RMS=7.3$ nm); b) after 12-th correction ($P-V=7.3$ nm, $RMS=0.6$ nm).



Fig. 33. Photograph of the multilayer spherical mirror for 13.5 nm wavelength in the frame. Diameter of the working aperture is 130 mm.

In spite of a greater wavelength of the traditional deep ultraviolet lithography (193 nm), because of a great number of lens and high requirements for the quality of the projective objectives, the methods of correction and certification with a subnanometer accuracy described in this article are urgent for the refracting optics too. In connection with this the researches on etching of fused quartz surfaces by ion beams with a compensated charge have been carried out. As well as in the case of metal surfaces, the main attention was given to the etching rate, to the reproducibility of the etching process and to the surface microroughness depending on the beam characteristics, incidence angles and material removal depths.

In Fig. 34 the dependences of quartz etching depth on the etching dose are presented. The dashed lines in the figure correspond to linear approximations of the dependencies. The ion energy was 200 and 300 eV, the grazing incidence angle was 42° . The comparison with similar dependences for Cr/Sc, Fig. 31, shows that the etching rate of fused quartz is almost twice as much. No nonlinearity at the initial stage of the etching is observed, that on the one hand, proves the hypothesis about the effect of the oxide layer in the case of Cr/Sc material and on the other hand, essentially facilitates the correction process.

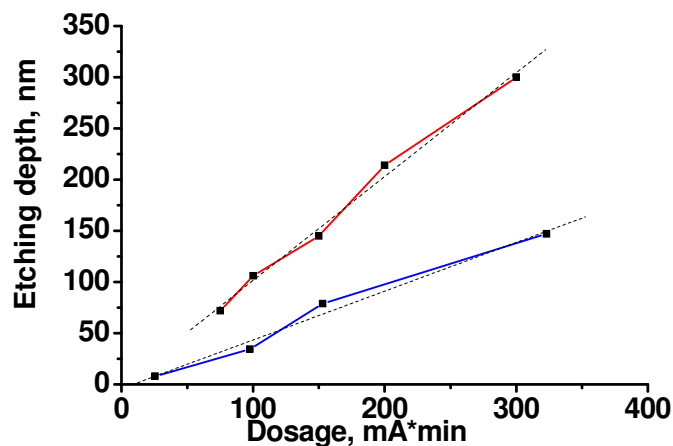


Fig. 34. Dependences of the etching depth on the dose for fused quartz. Etching is performed by argon ions with compensated charge and with energy $E_i = 200$ and 300 eV; - - - linear approximation of dependences.

The data on the surface roughness of a fused quartz substrate etched by ions (neutrals) with energies of 200 and 300 eV, for various removal depths, measured by means of the atomic-force microscope and by x-ray diffractometry are presented in table 1. The substrates manufactured by General optics (USA) were used in the experiment. The minimal roughness of initial surfaces measured with an atomic-force microscope was 0.13 nm, and with the x-ray reflection it was about 0.4 nm. From the table it is evident that atomic-force microscope measurements have shown a weaker influence of the etching process on the surface roughness, in comparison with the roughness measurements made by the x-ray diffractometry method. A more detailed discussion of this difference is beyond the given article.

Thus, the presented experimental data show that these technologies of vacuum deposition and ion-beam etching in the aggregate allow to correct with a subnanometer accuracy the surface shape of optical elements practically of any materials (metals, dielectrics, semiconductors) with keeping the surface on a supersmooth level. This technology is

suitable for manufacturing elements for imaging x-ray optics, and for high resolution systems in visible and deep ultra-violet ranges.

Energy of neutrals in the beam, eV	Etching depth, nm	Etching rate, nm/min	Roughness, nm	
			AFM	X-ray
200	30	7.90	0.13	0.40
200	79	7.90	0.15	0.60
200	157	7.85	0.18	0.65
200	237	7.90	0.20	0.70
300	353	11.70	0.28	1.0
Initial surface roughness, nm			0.13	0.40

Table 1. Roughness of fused quartz substrates depending on neutral (ion) energy and etching depths measured by atomic-force microscopy (AFM) and x-ray diffractometry (X-ray) methods.

8. Reflecting multilayer interference mirrors

The final stage of manufacturing a precise mirror for ultrahigh resolution imaging x-ray optical systems is the procedure of the deposition of multilayer reflecting coating on a substrate. A low polarizability of materials ($\epsilon \leq 1$) and correspondingly a small jump of the refraction factor $\Delta n = 0.0001 - 0.1$ on the vacuum-material interface and a strong absorption of the radiation by all materials completely exclude the application of refractive optics in the extreme ultra-violet and soft x-ray ranges.

Because of a low reflection from one interface the reflection optics of normal incidence can be only interferential and the number of layers demanded for the achievement of a high reflectivity depending on a wavelength can reach a value of $10^2 - 10^3$.

The absorption of the radiation in multilayer structures leads to the fact that the reflectivity is always less than unity. While choosing an optimal pair of materials providing a maximal reflectivity on a given wavelength the circumstance is often used that in the range of wavelengths directly adjoining the absorption edge of the material, $\lambda > \lambda_{AE}$ (λ_{AE} is the wavelength of the material absorption edge) and coinciding with an anomalous dispersion of the optical constants the lowest absorption and the maximal polarizability of materials are observed. For some materials in the field of *K*- and *L*- absorption edges the refraction factor can even exceed unity. In Fig. 35 the calculated spectral dependences of the maximal reflection coefficients for the most attractive pairs of materials in a spectral range of 3 - 16 nm, representing the biggest interest for projection nanolithography and high resolution x-ray microscopy are shown.

The greatest experimental reflectivity, about 70 %, was obtained at a wavelength of 13.5 nm. The spectral range around $\lambda \approx 6.7$ nm (area of boron anomalous dispersion) is of interest for projection x-ray lithography. However the reflectivity obtained here with *La/B₄C* multilayer mirrors at a normal angle of incidence does not exceed 45-47 % (Andreev et al., 2009) that is not enough for lithographic applications.

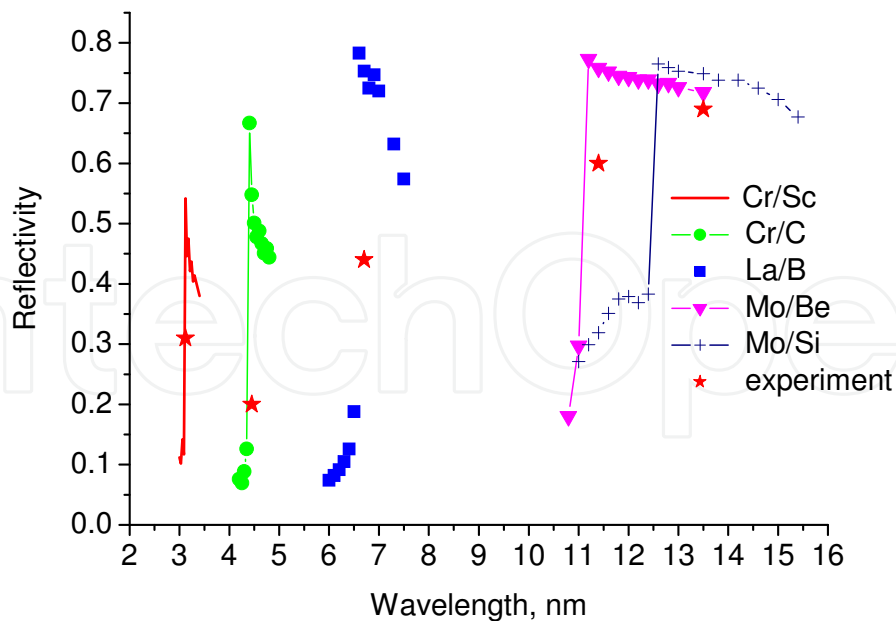


Fig. 35. Calculated (lines with symbols) and experimental (stars, (Website ESRF, 2006; Andreev et al., 2003)) reflection coefficients of mostly attractive pairs of materials in X-ray and EUV ranges.

On the short-wave length side the working wavelength of the normal incidence multilayer optics is limited by technology capabilities for depositing high-quality short period multilayer structures. At present the shortest periods have multilayer structures based on W/B_4C (the period $d \approx 1$ nm) (Vainer et al., 2006; Platonov, 2002) and Cr/Sc ($d \approx 1.5$ nm) (Salashchenko & Shamov, 1997; Website ESRF, 2006).

A number of special requirements are imposed on the multilayers which should be deposited onto substrates for imaging optics. In particular, to provide a constructive interference of the waves reflected from different interfaces, the radiation wavelength λ , the local angle of incidence $\theta(\vec{r})$ and the period of the multilayer structure $d(\vec{r})$ should satisfy the Bragg condition

$$d(\vec{r}) = \frac{\lambda}{2 \sin \theta(\vec{r})}, \quad (11)$$

where \vec{r} is a radius-vector of a point of incidence of the radiation on the structure. As the incidence angles are a function of the coordinates it results in the necessity to deposit multilayer structures with a variable over the surface period, so-called "graded" structures. In some cases, for example, when the angular divergence of the X-ray beam falling on one point of the mirror surface exceeds the Bragg's peak width, the multilayer structure should have a variable period on depth (Kozhevnikov et al., 2001).

One more important feature of multilayer structures for precise optics can be explained as follows. For multilayer dispersive elements the maximum deviation of the local value of the period δd from the nominal one is determined by the condition of synchronism of the waves reflected from various interfaces which can be expressed through the spectral selectivity of a mirror $S = \delta \lambda / \lambda = \delta d / d \approx 1 / N$ (N is a number of periods). In the case of precision multilayer imaging optics when the required surface shape accuracy is at a subnanometer

level to the synchronism condition an extra requirement for the preservation of the mirror surface shape is added. For example, for the well-known *Mo/Si* multilayer structure, optimized on the wavelength of $\lambda=13.5$ nm, the period is $d\approx 7$ nm at a number of periods $N\approx 40$. Correspondingly the general thickness of the structure is $L=N\cdot d=280$ nm. The local error of the period of 1 % will affect weakly on reflectivity, however the surface shape of the mirror will produce a change of 2.8 nm, which already can essentially produce an influence on imaging properties of the mirror.

From these simple estimations two important conclusions follow. Firstly, when designing and manufacturing the surface shape of a substrate it is necessary to take into account the real thickness of a multilayer coating which would be deposited onto the substrate. Secondly, it is necessary to provide a high, at a level of 0.2-0.3 %, accuracy of local values of the period over the mirror surface. Besides, an intrinsic stress in the multilayer structures, which can also deform the surface shape, must be taken into account. The estimation of the deformation δx of a substrate with a diameter D , a thickness h_{sub} , with the Yung modulus E and the Poisson factor ν on which a h_f thick film with the intrinsic stress σ is deposited, can be performed by means of equations

$$\delta x = \frac{3 \cdot \sigma \cdot h_f}{4 \cdot Y} \cdot \frac{D^2}{h_{sub}^2}, \quad (12)$$

$$Y = \frac{E}{1 - \nu}$$

For instance, for optimized on maximum of the reflection coefficient *Mo/Si* multilayer structure (portion of *Mo* layer in the period $\gamma=d_{Mo}/(d_{Mo}+d_{Si}) = 0.4$) the stress in our case is about $\sigma = -350$ MPa (Fig. 36). At deposition of such a multilayer structure (general thickness is $L=N\cdot d=280$ nm) on a substrate of fused quartz with the diameter $D=220$ mm and thickness $h=50$ mm ($Y=84,4$ ГПа) the maximal deformation of the substrate surface would be about 17 nm, that essentially exceeds an admissible level of the surface shape deformation of a mirror for EUV lithography.

Different groups solve this problem in different ways. One the solution is the use of mirrors with a specified thickness ratio of molybdenum layer in the periods $\gamma_{Mo} \approx 0.5 - 0.7$ when the stress is close to zero (Windt et al., 1994; Zoethout et al., 2003). The other solution consists in adding a third material into the periods, for example *Ru* (Oshino et al., 2003). However, all these methods, either because of a stronger absorption of EUV radiation or because of an interface roughness growth have smaller, of 10-20 %, absolute values of the reflectivity.

In IPM RAS a technique of the stress compensation based on the use of special sublayers lying under the basic *Mo/Si* multilayer structure is under development. For *Cr/Sc* multilayer structures the stress is close to zero at $\gamma_{Cr}=d_{Cr}/(d_{Cr}+d_{Sc})\approx 0.5$ (Fig. 37 (Andreev et al., 2005)). At $\gamma_{Cr}>0.5$ a sign of the stress is positive on the contrary to the *Mo/Si* structures at $\gamma_{Mo}= 0.4$, when it is negative. The total stress σ_{eff} in the structure consisting of *Cr/Sc* and *Mo/Si* multilayer films, can be determined from a ratio

$$\sigma_{eff} = \frac{[(\sigma_{Mo/Si} \cdot d_{Mo/Si} \cdot N_{Mo/Si}) + (\sigma_{Cr/Sc} \cdot d_{Cr/Sc} \cdot N_{Cr/Sc})]}{(d_{Mo/Si} \cdot N_{Mo/Si}) + (d_{Cr/Sc} \cdot N_{Cr/Sc})}, \quad (13)$$

from which it follows, that optimizing the composition and the thickness of *Cr/Sc* layers it is possible to compensate the stress in the basic *Mo/Si* reflecting multilayer structure.

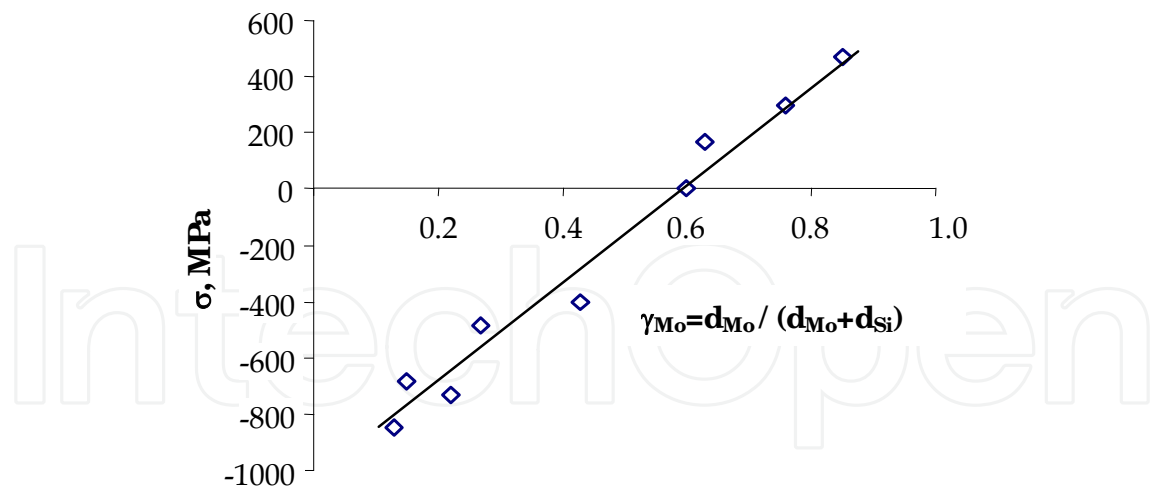


Fig. 36. Stress in *Mo/Si* multilayer structures depending on ratio of *Mo* layer in period $\gamma_{Mo} = d_{Mo} / (d_{Mo} + d_{Si})$ at fixed period $d = 6.97$ nm.

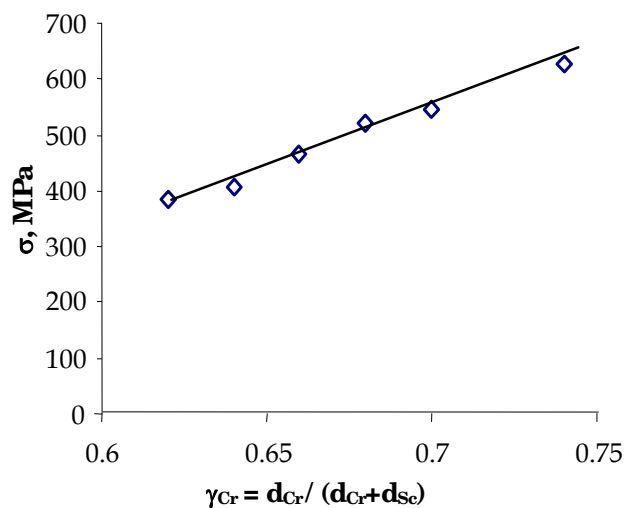


Fig. 37. Stress in *Cr/Sc* multilayer structure depending on ratio of *Cr* layer in period $\gamma_{Cr} = d_{Cr} / (d_{Cr} + d_{Sc})$ at fixed period $d = 5.4$ nm.

In practice it is necessary to consider a process of the stress relaxation which, depending on the structure and materials, is variable over several days. Totally the stress can change by tens percent. An example of such a process is illustrated in Fig. 38 in which the time dependencies of the stress in multilayer structures consisting of anti-stress *Cr/Sc* sublayers and *Mo/Si* reflecting layers are presented. The structures differ by thicknesses of the sublayers.

It is necessary to note, that the stress value is affected not only by ratio of the layer thickness in the period, but also by the period size and conditions in which the films were deposited.

For depositing multilayer structures a method of magnetron sputtering is used in IPM RAS. The method allows depositing films onto curved as well as flat substrates. The conditions, under which multilayer structures are deposited, are briefly described in section 6, devoted to the correction of the substrate surface shape by the method of local thin-film deposition. The facilities have from two to six magnetron sources that allows depositing at one technological cycle reflecting, anti-stress and anti-diffusion barrier layers. Now the

technologies of depositing more than twenty various pairs of materials are developed. It allows manufacturing optics for a whole x-ray and extreme ultra-violet spectral range. More details about the properties of the multilayer structures can be found in (Andreev et al., 2003).

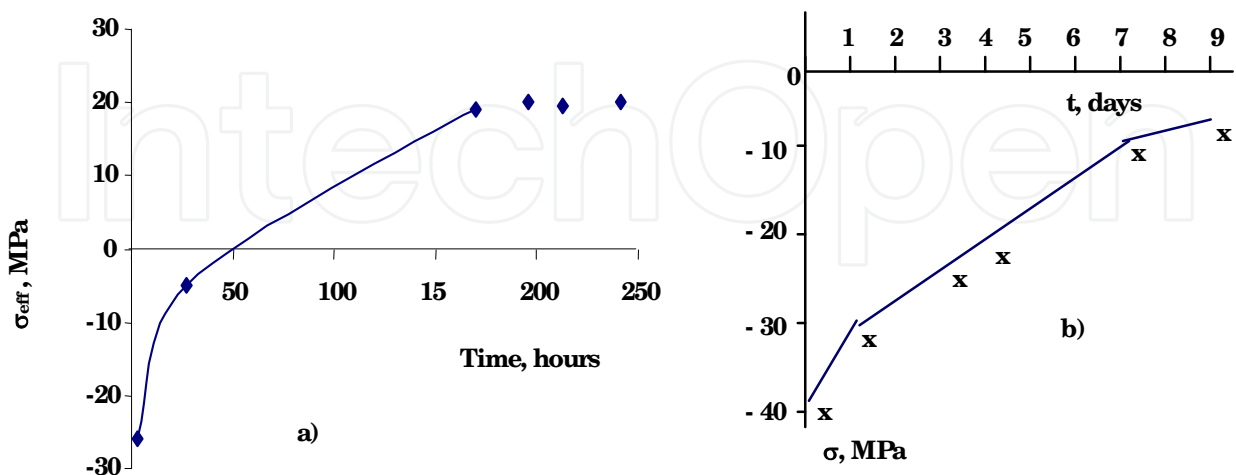


Fig. 38. Stress in *Mo/Si* multilayer structures with anti-stress *Cr/Sc* sublayers versus of time.
 a) - [(*Cr/Sc*) \times 42; $d=5.38$ nm; $\gamma=0.67$ / (*Mo/Si*) \times 45; $d=6.98$ nm; $\gamma=0.4$] and
 b) - [(*Cr/Sc*) \times 40; $d=5.38$ nm; $\gamma=0.67$ / (*Mo/Si*) \times 45; $d=6.98$ nm; $\gamma=0.4$].

A great volume of works, high requirements for the coating quality and for accuracy of the period distribution over a substrate surface dictate the need for an operative information about characteristics of the deposited coatings with the purpose of correcting the technological process. It is most convenient to perform such work with the presence of laboratory reflectometers, allowing the investigation of multilayer structures on working wavelengths and located in the immediate vicinity of technologists. Therefore laboratory reflectometers are constantly being developed and improved recently. In Refs. (Loyen et al., 2003; Miyake et al., 2003; Gulikson et al., 1992) the specialized reflectometers for investigating multilayer optics in the range around 13.5 nm are described. As a source of the soft x-ray and EUV radiation the laser plasma is used, which arises due to the irradiation of solid-state targets by laser light with a power density about 10^9 W/cm². For monochromatization the radiation spherical diffraction gratings operating at grazing angles are used. The characteristic fluxes of the photons in the working range of wavelengths of 10-16 nm on the investigated samples with the probe beam size ≈ 2 mm are 10^7 - 10^8 photons / (0.1 nm \times s). The results of reflectivity measurements of *Mo/Si* multilayer mirrors in the area of 13.5 nm obtained with the help of these reflectometers as compared with the data obtained with a PTB-reflectometer (synchrotron BESSY-2, Berlin, Germany, which is considered as the reference one), have shown the coincidence of the measured reflection coefficients at a level of 3 % and the resonant wavelength ≈ 0.01 nm.

The basic disadvantages of these reflectometers, in our opinion, are a narrow range of working wavelengths and a low spectral resolution caused by the applied monochromator scheme. The monochromator consists of two stationary slits and spherical (or toroidal) diffraction grating. Scanning across the spectrum is carried out due to the diffraction gratings rotation around its axis. According to this arrangement, the position of the slits and the diffraction grating coincides with the Rowland circle (Rowland, 1893) only for one

wavelength that essentially limits the range where the spectral resolution of the monochromator is kept at the acceptable level of $\Delta\lambda_{app} \approx 0.01-0.02$ nm. The other factor limiting working spectral range of the reflectometer is the type of the used radiation source (laser plasma) which large size does not allow scanning by the entrance slit of the grating spectrometer.

Our group develops multilayer optics for a wide spectral range $\lambda=0.6-50$ nm and the monochromator spectral resolution up to 0.003-0.005 nm is frequently required. Therefore in IPM RAS laboratory reflectometers on the basis of high resolution grating monochromators have been developed. These monochromators have a movable entrance slit and diffraction grating (Chkhalo et al., 1998; Zuev & Mitrofanov, 2002; Bibishkin et al., 2004; Bibishkin et al., 2005). In the reflectometers the monochromators of type RSM-500 (Lukirsky et al., 1967) and McPherson-247 (Website Mcpherson Company, 2009) are used. The photograph and optical scheme of the last generation reflectometer are given in Fig. 39. Owing to such a spectrometer the kinematic scheme slits and diffraction grating are always located in the Rowland focusing circle so that the high spectral resolution of the device in the whole range of wavelengths is provided. Two diffraction gratings with various radiuses of curvature cover this spectral range.

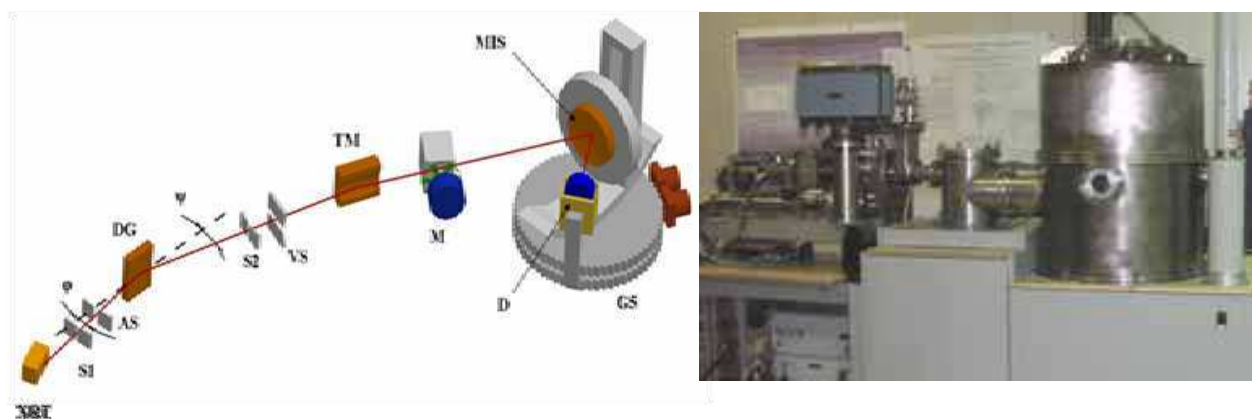


Fig. 39. Optical scheme and photograph of the reflectometer. XRT - x-ray tube; S1, S2 - entrance and exit slits; AS, VS - horizontal and vertical anti-scattering slits; DG - diffraction grating; TM - toroidal mirror; M - probe beam intensity monitor; MIS - investigated sample; D - detector; G5 - five-axes goniometer.

In the reflectometer the radiation from the anode of the x-ray tube (XRT) through the entrance slit of the monochromator (S1) falls on the diffraction grating (DG). The diffracted monochromatic radiation according to the diffraction grating equation $\cos\varphi - \cos\psi = m\lambda/D$ (m - the order of diffraction, λ - a wavelength and D - the grating period, φ and ψ angles of diffraction and incidence, correspondingly) is focused onto the spectrometer exit slit S2. Scanning across the spectrum is carried out by linear moving of the diffraction grating and the exit slit, with a simultaneous turn of the diffraction grating so that the condition $X_l = R_g \cdot \sin\psi$, where R_g - radius and X_l - distance between the diffraction grating center and the exit slit is satisfied. An anti-scattering diaphragm (AS) reduces the intensity of scattered radiation at the output of the monochromator and limits the irradiated area of the diffraction grating. The monochromatic radiation by means of a toroidal mirror (TM) is focused on the investigated sample. The other important function of the toroidal mirror is connected with a filtration of higher diffraction orders which is especially urgent when

working with bremsstrahlung of the tungsten anode. Radiuses of the toroidal mirror are chosen in such a way that in a horizontal plane the exit slit and in a vertical plane the source are imaged on the sample under study.

The studied sample is installed on a five-axis goniometer which photograph and scheme of movements are shown in Fig. 40. The linear translation along X and Z axes, the rotation around them (ω and φ) and the inclination θ , allow to insert any point of the sample under study with a diameter up to 300 mm into the x-ray beam. The detector executes 2φ rotation. The additional inclination of the detector 2θ allows to increase the numerical aperture of the sample which can be tested up to $NA=0.5$.

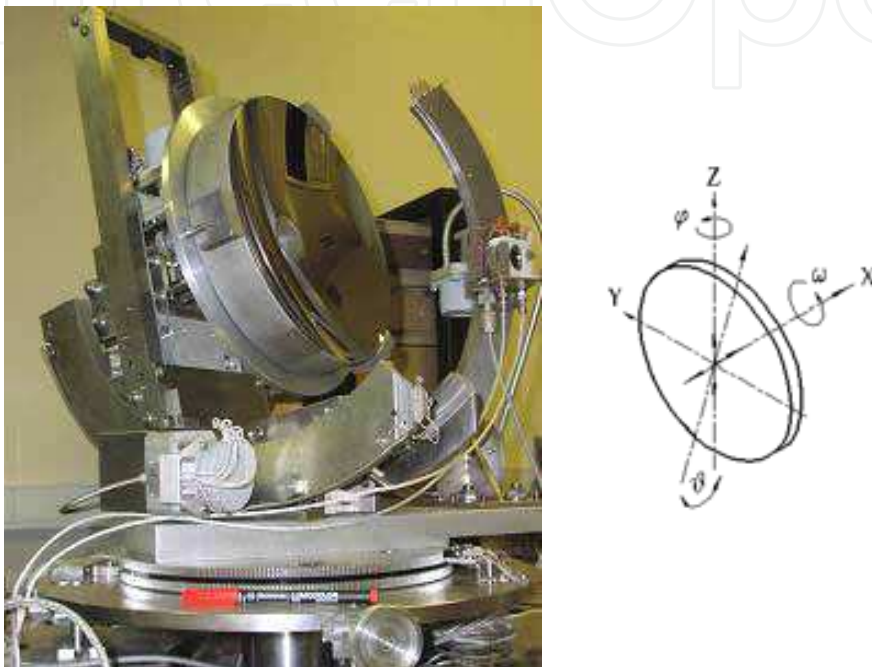


Fig. 40. Photograph of the goniometer and scheme of movements provided by the goniometer.

The concept of a spectrometer-monochromator with a movable slit and diffraction grating became possible only due to the application of the dismantlable x-ray tube of an original design as the radiation source. The advantages of classical sealed x-ray tubes are their small dimensions and weight, simplicity in operation, sufficient for reflectometric applications intensity of the x-ray radiation, and long life-time. However the application of these sources for precision reflectometry in soft x-ray and extreme ultra-violet ranges has shown that because of the fast contamination of the anode by products of thermocathode material erosion and hydrocarbons decomposition under a powerful electron-beam, emission characteristics and life-time of the tubes collapsed when comparing with expected values.

For solving this problem in our work the tube was equipped with an ion-beam source for cleaning anodes from contaminations (Bibishkin et al., 2003). It allows to work without opening the spectrometer and the tube to the atmosphere within several months thus approaching its operation mode to the traditional sealed X-ray tubes for hard X-rays. The work is done on K , L and M characteristic lines of target (anode) materials and on continuous bremsstrahlung spectrum of tungsten. On one holder about 8 targets of various materials are installed. It is necessary to note, that frequently it is possible to use a few spectral lines from one target.

As an illustration in Fig. 41 the measured spectral dependence of reflectivity of *Mo/Si* multilayer spherical mirror shown in Fig. 40 is presented. The measurement has been performed with the reflectometer at an incidence angle of the radiation to the sample of 5° (from the local normal).

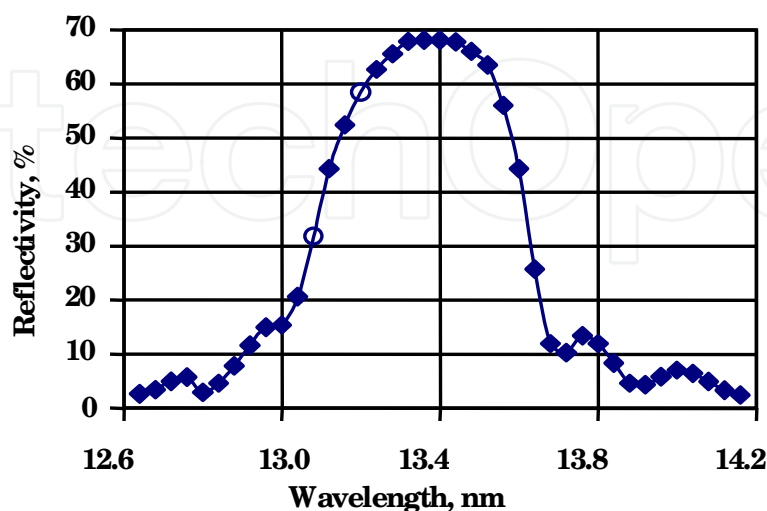


Fig. 41. Spectral dependence of the reflection coefficient of *Mo/Si* multilayer mirror deposited onto spherical substrate. Angle of incidence was 5° from the local normal.

One more important advantage of the x-ray tube as a source of X-ray radiation is that in the field of wavelengths $\lambda < 3$ nm because of aberrations of spherical grating the spectral width of the probe beam is $\Delta\lambda_G \geq 0.01$ nm while the spectral resolution of short period multilayers reaches values $\Delta\lambda_{MIS} < 0.01$ nm. Since the natural width of characteristic lines of some materials in this range is essentially less than this value this circumstance provides precision measurements of reflective characteristics of multilayer mirrors, even when monochromator does not provide the demanded resolution.

Thus, the developed in IPM RAS methods of multilayer coating deposition, stress compensation in the film structures, laboratory metrology of the mirrors at working wavelengths, restoration of the substrates without any damage of the substrate surface shape and roughness allow us to make and certify high reflecting multilayer mirrors with a sub-nanometer level surface shape accuracy attended for super-high resolution imaging X-ray optics.

9. Conclusion

In the given article the basic researches and the full cycle of developed in IPM RAS technologies and metrology techniques, from the substrate surface shape correction to the deposition of multilayer coatings on them which are required for manufacturing high reflecting mirrors for diffraction quality imaging in the extreme ultra-violet and in the soft X-ray ranges are described. As a whole, it is evident that the problem of manufacturing such optics for high resolution EUV lithography and X-ray microscopy is already solved as a first approximation. The further activity should be directed toward the increase of both in manufacturing accuracy of optical surfaces up to a level of $RMS=0.1$ nm and in the numerical aperture of objectives up to $NA=0.4-0.6$.

In this connection upgrading the interferometric methods for surface shape measurements of optical elements and wave-front deformations of objectives, first of all, and regarding the increase of their working numerical aperture is a subject of current interest. The diffraction interferometers utilizing the tipped fiber as a source of the reference spherical wave look rather attractive. Owing to the simplicity of the design, high intensity of the diffracted wave, weak sensitivity to the adjustment in an optical circuit and a number of other advantages the interferometers which are simple in operation can be developed for the optical industry. In the framework of the given article the problem, arising when aspherical surfaces are under investigation, of development and optimization of correctors transforming the reference spherical fronts into the aspherical ones which shapes are identical to the shapes of the studied surfaces was not practically discussed. Meanwhile, traditional lens null-correctors have limited capabilities, rather complicated in manufacturing and expensive and demand complicated calibrating procedures for taking into account the wave-front distortions due to errors of the corrector itself. In this connection diffraction correctors represent a significant interest (Akatov et al., 2004).

A gross potential for the surface shape correction of dielectric materials by means of ion-beams has RF-etching in chemically active environments. The first experiments on etching of quartz substrates by means of the RF-etching have shown that the surface micro-roughness did not change down to the removal depths of a few micrometers (Akhsakhalyan et al., 2008).

The most serious problem on the way of manufacturing the effective optics for the soft X-ray radiation, $\lambda < 10$ nm, is that reflection coefficients of the multilayer mirrors are not sufficiently high. Nevertheless, the results that have been recently obtained in the field of the X-ray optics teams may be considered as a break-through because they lay the foundation of developing such important physico-technological directions as projection EUV nanolithography, X-ray microscopy and extraterrestrial astronomy of the ultrahigh resolution.

10. References

- Akhsakhalyan, A.D.; Vainer, Yu.A.; Volgunov, D.G.; Drozdov, M.N.; Kluev, E.B.; Kuznetsov, M.I.; Salashchenko, N.N.; Kharitonov, A.I. & Chkhalo, N.I. (2008). Application of reactive ion-beam etching for surface shape correction of X-ray mirrors, Proceedings of Workshop "X-ray optics - 2008", pp. 26-28, Chernogolovka, Moscow region, 6-9 October 2008, p. 26-28, IPTM, Chernogolovka. (in Russian)
- Allen, L.N.; Keim, R.E. & Lewis, T.S. (1991). Surface error correction of a Keck 10 m telescope primary mirror segment by ion figuring, Proceedings SPIE, Vol. 1531, 1991, pp. 195-204.
- Andreev, S.S.; Bulgakova, S.A.; Gaponov, S.V.; Gusev, S.A.; Zuev, S.Yu.; Kluev, E.B.; Luchin, V.I.; Lopatin, A.Ya.; Mazanova, L.M.; Prokhorov, K.A.; Sadova, E.N.; Salashchenko, N.N. & Shamov, E.A. (2000). Investigations in field of projection lithography of extreme ultraviolet region in Institute for physics of microstructures RAS, Surface. X-ray, synchrotron and neutron investigations, Vol. 1, 2000, pp. 32-41. (in Russian)
- Andreev, S.S.; Akhsakhalyan, A.D.; Bibishkin, M.S.; Chkhalo, N.I.; Gaponov, S.V.; Gusev, S.A.; Kluev, E.B.; Prokhorov, K.A.; Salashchenko, N.N.; Schafers, F. & Zuev,

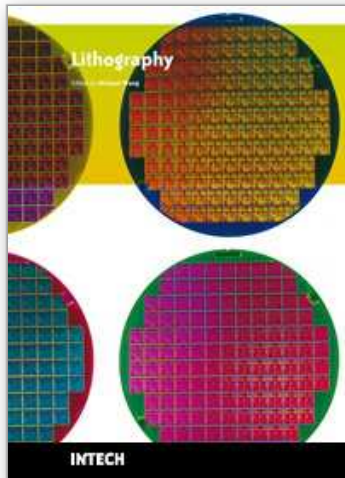
- S.Yu. (2003). Multilayer optics for XUV spectral region: technology fabrication and applications, *Central European Journal of Physics*, Vol. 1, 2003, pp. 191-209.
- Adreev, S.S.; Kluev, E.B.; Misinov, A.L.; Polkovnikov, V.N.; Salashchenko, N.N.; Suslov, L.A. & Chernov, V.V. (2005). Compensation of elastic deformation of Mo/Si multilayer structures on quartz and zerodur substrates using buffer Cr/Sc technique, *Surface investigations*, Vol. 2, 2005, pp. 45-48. (In Russian)
- Andreev, S.S.; Barysheva, M.M.; Chkhalo, N.I.; Gusev, S.A.; Pestov, A.E.; Polkovnikov, V.N.; Salashchenko, N.N.; Shmaenok, L. A., Vainer, Yu.A. & Zuev, S.Yu. (2009). Multilayered mirrors based on La/B₄C(B₉C) for x-ray range near anomalous dispersion of boron (λ near 6.7 nm), *Nuclear Instruments and Methods in Physics Research Sec.A*, Vol. 603, 2009, pp. 80-82.
- Archer, K.M. (1997). Craniofacial reconstruction using hierarchical b-spline interpolation", A thesis submitted in partial fulfilment of the requirements for the degree of master of applied science, The university of British Columbia, 1997, p. 113.
- Asadchikov, V.E.; Kapabekov, A.Yu.; Kozhevnikov, I.V.; Levashov, V.E. & Sagitov, S.I. (1998). Experimental investigation of roughness correlation of a film and a substrate by means of X-ray scattering, *Crystallography*, Vol. 43, No. 1, 1998, pp. 119-130. (In Russian)
- Barbee, T.W. (Jr.) (1981). Sputtered layered synthetic microstructures (LSM) dispersion elements, *Proceedings of Conference "Low energy X-ray diagnostics"*, pp. 131-145, Monterey, USA, 1981, N. Y.: Amer. Inst. Phys.
- Benschop, J.P.H.; Kaiser, W.M. & Ockwell, D.C. (1999). EUCLIDES, the European EUVL program, *SPIE Symposium on Micro-lithography*, Vol. 3676, 1999, p. 246.
- Bibishkin^a, M.S.; Zabrodin, I.G.; Klyuenkov, E.B.; Salashchenko, N.N.; Chekhonadskih, D.P. & Chkhalo, N.I. (2003). A new dismountable tube for soft X-ray radiation, *Surface investigations*, No. 2, 2003, pp. 41-45. (In Russian)
- Bibishkin^b, M.S.; Zuev, S.Yu.; Salashchenko, N.N. & Chkhalo, N.I. (2003). Measuring of microroughness of surfaces using soft X-ray radiation, *Surface investigations*, No. 1, 2003, pp. 94-96. (In Russian)
- Bibishkin, M.S.; Chekhonadskih, D.P.; Chkhalo, N.I.; Klyuenkov, E.B.; Pestov, A.E.; Salashchenko, N.N.; Shmaenok, L.A.; Zabrodin, I.G. & Zuev, S.Yu. (2004). Laboratory methods for investigation of multilayer mirrors in Extreme Ultraviolet and Soft X-Ray region, *Proceedings of SPIE*, Vol. 5401, 2004, pp. 8-15.
- Bibishkin, M.S.; Vainer, Yu.A.; Pestov, A.E.; Prokhorov, K.A.; Salashchenko, N.N.; Fraerman, A.A. & Chkhalo, N.I. (2005). Investigation of characteristics of multilayer X-ray mirrors with ultra-short periods $d = 0,7-2,4$ nm, *Bulletin of the Russian Academy of Sciences: Physics*, Vol. 69, No. 2, 2005, pp. 199-206.
- Blunt, R. (2006). White light interferometry - a production worthy technique for measuring surface roughness on semiconductor wafers, *Proceedings of CEMANTECH Conference*, pp. 59-62, Vancouver, Canada, April 24-27, 2006.
- Born, M. & Wolf, E. (1973). *Principles of optics*, second edition, Science, Moscow. (In Russian)
- Braat, J. (1987). Polynomial expansion of severely aberrated wave fronts, *Optical Society of America*, Vol. 4, No. 4, 1987, pp. 643-650.
- Chason, E. & Mayer, T. M. (1993). Low energy ion bombardment induced roughening and smoothing of SiO₂ surfaces, *Applied Physics Letters*, Vol. 62, No. 4, 1993, pp. 363-365.
- Cheng, P. (1987). *Instrumentation and Biological Applications*, In *X-ray Microscopy*, Springer Verlag.

- Chkhalo, N.I.; Dolbnya, I.G.; Fedorchenko, M.V.; Kruglyakov, E.P.; Zarodyshev, A.V. & Zolotarev, K.V. (1993). Multilayer mirror on copper-nickel substrates for intense X-ray beams. Proceedings of the 4-th International Conference "X-Ray Microscopy 4", pp. 586-592, Russia, Chernogolovka, September 20-24, 1993, IPTM, Chernogolovka.
- Chkhalo, N.I.; Fedorchenko, M.V.; Kruglyakov, E.P.; Volokhov, A.I.; Baraboshkin, K.S.; Komarov, V.F.; Kostyakov, S.I. & Petrov, E.A. (1995). Ultradispersed diamond powders of detonation nature for polishing X-ray mirrors, Nuclear Instruments and Methods in Physics Research A, Vol. 359, 1995, pp. 155-156.
- Chkhalo, N.I.; Kirpotin, A.N.; Kruglyakov, E.P. & Semenov, E.P. (1998). Reflectometer for precision tests of optical components in the ultrasoft X-ray range, Nuclear Instruments and Methods in Physics Research. A, Vol. 405, 1998, pp. 393-395.
- Chkhalo^a, N.I.; Raskin, D.G. & Salashchenko, N.N. (2008). Capabilities of microinterferometer with digital recording of images for studying micro-objects with sub-nanometer resolution, Proceedings of SPIE, Vol. 7025, 2008, p. 702512.
- Chkhalo^b, N.I.; Dorofeyev, I.A.; Salashchenko, N.N. & Toropov, M.N. (2008). A plane wave diffraction on a pin-hole in a film with a finite thickness and real electrodynamic properties, Proceedings of SPIE, Vol. 7025, 2008, p. 702506.
- Chkhalo^c, N.I.; Klimov, A.Yu.; Rogov, V.V.; Salashchenko, N.N. & Toropov, M.N. (2008). A source of a reference spherical wave based on a single mode optical fiber with a narrowed exit aperture. Rev. Sci. Instrum., Vol. 79, 2008, p. 033107.
- Chkhalo^d, N.; Paramonov, L.; Pestov, A. ; Raskin, D. & Salashchenko, N. (2008). Correction of the EUV mirror substrate shape by ion beam, Proceedings of SPIE , Vol. 7025, 2008, p. 702503.
- Dinger, U.; Bisert, F.; Lasser, H.; Mayer, M.; Seifert, A. ; Seitz, G.; Stacklies, S.; Stickel, F.-J. & Weise, M. (2000). Mirror substrates for EUV-lithography: progress in metrology and optical fabrication technology, Proceedings of SPIE, Vol. 4146, 2000, pp. 35-46.
- Dorofeyev, I.; Jersch, J. & Fuchs, H. (2003). Spectral composition of electromagnetic fluctuations induced by a lossy layered system, Annalen der Physik, Vol. 12, No. 7-8, 2003, pp. 421-437.
- Dorofeyev, I. (2009). Amplitude-phase characteristics of electromagnetic fields diffracted by a hole in a thin film with realistic optical properties, Physica E, Vol. 41, 2009, pp. 762-770.
- Drozдов, M.N.; Drozdov, Yu.N.; Barysheva, M.M.; Polkovnikov, V.N. & Chkhalo, N.I. (2009). Minimization of matrix effects upon layer-by-layer analysis of multilayer metallic nanostructures La/B4C by SIMS using cluster secondary ions, Proceedings of Symposium "Nanophysics and nanoelectronics", Vol. 1, pp. 190-191, Nizhniy Novgorod Russia, 16-20 March 2009, IPM RAS, Nizhniy Novgorod. (in Russian)
- Gavrilin, D.A. (2003). Investigations of methods for shape description of complicated optical surfaces at interferometrical control, Ph.D. thesis, St.-Petersburg, Russia, 103 p. (in Russian)
- Ghigo, M.; Canestrari, R.; Spiga, D. & Novi, A. (2007). Correction of high spatial frequency errors on optical surfaces by means of Ion Beam Figuring, Proceedings of SPIE, Vol. 6671, 2007, p. 667114.
- Goldberg, K.A. & Kevin, G. (2001). Wave-front measurement errors from restricted concentric subdomains, J. Opt. Soc. Am. A, Vol. 18, No. 9, 2001, pp.

- Goldberg, K.A.; Naulleau, P.; Bokor, J.; Chapman, H.N. & Barty, A. (2002). Testing extreme ultraviolet optics with visible-light and extreme ultraviolet interferometry, *J. Vac. Sci. Technol. B*, Vol. 20, No. 6, 2002, pp. 2834-2839.
- Griffith, J. E. & Grigg, D.A. (1993). Dimensional metrology with scanning probe microscopes, *Journal of Applied Physics*, Vol. 74, 1993, pp. R83-R109.
- Gullikson, E.M.; Underwood, J.H.; Batson, P.C. and Nikitin, V. (1992). A soft X-ray/EUV reflectometer based on a laser produced plasma source, *Journal of x-ray science and technology*, Vol. 3, 1992, pp. 283-299.
- Gwyn, C. (1998). White paper on Extreme ultraviolet Lithography, *Proceedings of EUV LLC*, 1998, Livermore.
- Klimov, A.Yu.; Rogov, V.V.; Salashchenko, N.N. & Chkhalo, N.I. (2008). A Spherical Wave Source Based on a Probe for a Near-Field Microscope, *Bulletin of the Russian Academy of Sciences: Physics*, Vol. 72, No. 2, 2008, pp. 204-206.
- Kluyenkov^a, E.B.; Pestov, A.E.; Polkovnikov, V.N.; Raskin, D.G.; Toropov, M.N.; Salashchenko, N.N. & Chkhalo, N.I. (2008). Testing and Correction of Optical Elements with Subnanometer Precision, *Nanotechnologies in Russia*, Vol. 3, Nos. 9-10, 2008, pp. 602-610.
- Klyuenkov^b, E.B.; Polkovnikov, V.N.; Salashchenko, N.N. & Chkhalo, N.I. (2008). Shape Correction of Optical Surfaces with Subnanometer Precision: Problems, Status, and Prospects, *Bulletin of the Russian Academy of Sciences: Physics*, Vol. 72, No. 2, 2008, pp. 188-191.
- Kozhevnikov, I.V.; Asadchikov, V.E.; Duparre, A.; Gilev, O.N.; Havronin, N.A.; Krivonosov, Yu.S.; Ostashov, V.I. & Steinert, J. (1999). Comparative study of the roughness of optical surfaces and thin films using atomic force microscopy, x-ray scattering and light scattering methods, *Proceedings of SPIE*, Vol. 3739, 1999, pp. 348-354.
- Kozhevnikov, I.V.; Bukreeva, I.N. & Ziegler, E. (2001). Nuclear Instruments and Methods in Physics Research Sec. A, Vol. 460, 2001, p. 424.
- Linnik, V.P. (1933). A simple interferometer to test optical systems, *Bulletin of the Academy of Science of the USSR*, Vol. 1, 1933, pp. 210-212.
- Loyen, L.; Bottger, T.; Braun, S.; Mai, H.; Leson, A.; Scholze, F.; Tummler, J.; Ulm, G.; Legall, H.; Nickels, P.V.; Sandner, W.; Stiel, H.; Rempel, C.; Schulze, M.; Brutscher, J.; Macco, F. & Mullender, S. (2003). A New Laboratory EUV Reflectometer for Large Optics using a Laser Plasma Source, *Proceedings of SPIE*, Vol. 5038, 2003, pp. 12-21.
- Lukirsky, A.P.; Brytov, I.A. & Komyak, N.I. (1967). Prototype of an X-ray spectrometer with diffraction grating and ionization detection for spectral region of 10-55 Å, *Apparatus and methods of X-ray analysis*, No. 2, 1967, pp. 4-19, L.: Engineering. (in Russian).
- Malacara, D., ed. (1992). *Optical shop testing*, 2nd ed., John Wiley & Sons, Inc., ISBN 0-471-52232-5, New York.
- Medecki, H.; Tejnli, E.; Goldberg, K.A. & Bokor, J. (1996). Phase-shifting point diffraction interferometer, *Optics letters*, Vol. 21, No. 19, 1996, pp. 1526-1528.
- Miyake, A.; Miyachi, T.; Amemiya, M.; Hasegawa, T.; Ogushi, N.; Yamamoto, T.; Masaki, F. & Watanabe, Y. (2003). LPP-based reflectometer for characterization of EUV lithography systems, *Proceedings of SPIE*, Vol. 5037, 2003, pp. 647-655.
- Murakami, K.; Saito, Y.; Ota, K. et al. (2003). Development of an experimental EUV interferometer for benchmarking several EUV wavefront metrology schemes, *Proceedings of SPIE*, Vol. 5037, 2003, pp. 75-82.

- Murakami, K.; Oshino, T.; Kondo, H.; Chiba, H.; Komatsuda, H.; Nomura, K. & Iwata, H. (2007). Development of optics for EUV lithography tools, *Proceedings of SPIE*, Vol. 6517, 2007, pp. 65170J.
- Naulleau, P.P.; Goldberg, K.A.; Lee, S.H.; Chang, C.; Attwood, D. & Bokor, J. (1999). Extreme-ultraviolet phase-shifting point-diffraction interferometer: a wave-front metrology tool with subangstrom reference-wave accuracy, *Appl. Opt.*, Vol. 38, No. 35, 1999, pp. 7252-7263.
- Naulleau, P.; Goldberg, K.A.; Lee, S.H.; Chang, Ch.; Atwood, D. & Bokor, J. (2000). The EUV phase-shifting point diffraction interferometer, *Synchrotron Radiation Instrumentation: Eleventh US National Conference*, ed. by P. Pianetta, p. 66-72, ISBN 1-56396-941-6, American Institute of Physics.
- Naulleau P.; Golberg K.A.; Anderson E.H. et. al. (2002). Sub-70 nm Extreme Ultraviolet Lithography at the Advanced Light Source Static Microfield Exposure Station Using the Engineering Test Stand Set-2 Optic, *Jour. Vac. Sci. Technol. B*, Vol. 20, 2002, pp. 2829-2833.
- Nevot, L. & Croce, P. (1980). Characterisation des surfaces par reflection rasante de rayon Application a l'etude du polissage de quelque verres silicates, *Revue de Physique Appliquee*, Vol. 15, 1980, pp. 761-779.
- Okatov, M.A.; Antonov, E.A.; Baigozhin, A. et al. (2004). *Handbook for optical-technologist*, St- Petersburg: Politechnica, 2004, 679 p.
- Oshino, T.; Shiraishi, M.; Kandaka, N.; Sugisaki, K.; Kondo, H.; Ota, K.; Mashima, K.; Murakami, K.; Oizumi, H.; Nishiyama, I. & Okazaki, S. (2003). Development of illumination optics and projection optics for high-NA EUV exposure tool (HiNA), *Proceedings of SPIE*, Vol. 5037, 2003, pp. 75-82.
- Ota, K.; Murakami, K.; Kondo, H.; Oshino, T.; Sugisaki, K. & Komatsuda, H. (2001). Feasibility study of EUV scanners, *Proceedings of SPIE*, Vol. 4343, 2001, pp. 60-69.
- Otaki, K.; Ota, K.; Nishiyama, I.; Yamamoto, T.; Fukuda, Y. & Okazaki, S. (2002). Development of the point diffraction interferometer for extreme ultraviolet lithography: Design, fabrication, and evaluation, *J. Vac. Sci. Technol B*, Vol. 20, No. 6, 2002, pp. 2449-2458.
- Palik, E.D. (1985). *Hanbook of optical constants of solids*, Naval Research Laboratory, Washington D.C., 1985, 749 pp.
- Parratt, L.G. (1954). Surface studies of solids by total reflection of x-rays, *Physical Review*, Vol. 35, 1954, pp. 359-369.
- Platonov, Yu.; Gomez, L. & Broadway, D. (2002). *Proceedings of SPIE*, Vol. 4782, 2002, p. 152.
- Protopopov, V.V.; Valiyev, K.A. & Imamov, R.M. (1999). Measurement of spatial distribution of superpolished surface roughness and defects in multilayer X-ray mirrors, *Surface investigations*, No. 1, 1999, pp. 111-119. (In Russian)
- Puryaev, D.T. (1976). *Methods for control of aspherical surfaces*, M: Engineering, 1976, 13 p. (in Russian)
- Rodionov, S.A.; Przhevalinsky, L.I. & Shekhonin, A.A. (1974). Application of coefficients of interpolation polynomial for optical system aberrations presentation, *Bulletin of the USSR institutions of higher education: Instrument engineering*, Vol. 17, No. 10, 1974, p. 104. (in Russian)
- Rodionov, S.A. (1995). Mthematical apparatus for ptics control - general approach, *Optical journal*, No. 8, 1995, pp. 49-51.
- Rowland, H. (1893). Gratings in theory and practice, *Phil. Mag.*, Vol. 35, 1893, p. 397.
- Salashchenko, N.N. & Shamov, E.A. (1997). *Optics communication*, Vol. 134, 1997, p. 7.

- Salashchenko, N.N. (2001). Optical Element and Method for Recovering the Substrate, Patent DE 101 01 820 A1. 00074P.
- Sinha, S.K.; Sirota, E.B.; Garoff, S. & Stanley, H.B. (1988). X-ray and neutron scattering from rough surfaces, *Physical Rev. B.*, Vol .38, No.4, 1988, pp. 2297-2311.
- Sommargren, G.E. (1996). Diffraction methods raise interferometer accuracy, *Laser Focus World*, Vol. 8, 1996, p. 61-71.
- Soufli, R.; Spiller, E.; Schmidt, M.A.; Davidson, J.C.; Grabner, R.F.; Gullikson, E.M.; Kaufmann, B.B.; Mrowka, S.; Baker, S.L.; Chapman, H.N.; Hudyma, R.M.; Taylor, J.S.; Walton, Ch.C.; Montcalm, C. & Folta, J.A. (2001). Multilayer optics for an extreme ultraviolet lithography tool with 70 nm resolution, *Proceedings of SPIE*, Vol. 4343, 2001, pp. 51-59.
- Stone, V.W.; Jonas, A.M.; Nysten, B. & Legras, R. (1999). Roughness of free surfaces of bulk amorphous polymers as studied by x-ray surface scattering and atomic force microscopy, *Physical Rev. B.*, Vol. 60, No. 8, 1999, pp. 5883-5894 .
- Sun, X.; Chen, S. & Shen, Q. (1998). Geometric calibration of lens using B-spline surface fitting, *Wuhan University Journal of Natural Sciences*, Vol. 3, No. 4, 1998, pp. 440-442.
- Swantner, W. & Weng, W. C. (1994). Gram-Schmidt orthogonalisation of Zernike polynomials for general aperture shapes, *Applied optics*, Vol. 33, No. 10, 1994, pp. 1832-1837.
- Sweeney, D.W.; Hudyma, R.M.; Chapman, H.N. & Shafer, D. (1998). EUV optical design for a 100 nm CD imaging system, *Proceedings of SPIE*, Vol. 3331, 1998, pp. 2-10.
- Underwood, J.H. & Barbee (Jr.), T.W. (1981). Layered synthetic microstructures as Bragg diffractors for X-rays and extreme ultraviolet: theory and predicted performance, *Appl. Opt.*, Vol. 20, 1981, pp. 3027-3034.
- Vainer, Yu.A.; Pestov, A.E.; Prokhorov, K.A.; Salashchenko, N.N.; Fraerman, A.A.; Chernov, V.V. & Chkhalo, N.I. (2006). Analysis of Cross-Correlation of Interface Roughness in Multilayer Structures with Ultrashort Periods, *Journal of Experimental and Theoretical Physics*, Vol. 103, No. 3, 2006, pp. 346-353.
- Warburton, W.K.; Rek, Z.U. & Barbee (Jr.), T.W. (1987). Quality Investigation of multilayer covers for X-ray optics, In *X-ray optics and microscopy*, pp. 222-231, World, Moscow. (In Russian)
- Website ESRF. http://www.esrf.eu/events/conferences/past-conferences-and-workshops/pxrms06/Detailed-programm/12_gullikson.pdf
- Website GO Corporation. <http://www.goochandhousego.com/products/cat/3>
- Website Mcpherson Company. <http://www.mcphersoninc.com/spectrometers/xuhvvuvuv/xuhvvuvuv.htm>
- Website Platar Company. <http://www.orc.ru/~platar/P1R.html>
- Website Veeco Instruments. <http://www.veeco.com>
- Website Zygo Corporation. <http://www.zygo.com>
- Williamson, D.M. (1995). The elusive diffraction limit, *OSA Proceedings on Extreme Ultraviolet Lithography*, F. Zernike and D.T. Attwood eds., Vol. 23, 1995, pp. 68-76.
- Windt, D.L.; Brown, W.L.; Volkert, C.A. & Waskiewicz, W.K. (1994). *J. Appl. Phys.*, Vol 78, 1994, p. 2423.
- Zoethout, E.; Sipos, G.; van de Kruijs, R.W.E.; Yakshin, A.E.; Louis, E.; Mullender, S. & Bijkerk, F. (2003). Stress mitigation in Mo/Si multilayers for EUV lithography, *Proceedings of SPIE*, Vol. 5037, 2003, pp. 872-878.
- Zuev, S.Yu. & Mitrofanov, A.V. (2002). Measurements of parameters of optical elements for X-ray telescopes, *Surface investigations*, No. 1, 2002, pp. 81-83. (In Russian)



Lithography

Edited by Michael Wang

ISBN 978-953-307-064-3

Hard cover, 656 pages

Publisher InTech

Published online 01, February, 2010

Published in print edition February, 2010

Lithography, the fundamental fabrication process of semiconductor devices, plays a critical role in micro- and nano-fabrications and the revolution in high density integrated circuits. This book is the result of inspirations and contributions from many researchers worldwide. Although the inclusion of the book chapters may not be a complete representation of all lithographic arts, it does represent a good collection of contributions in this field. We hope readers will enjoy reading the book as much as we have enjoyed bringing it together. We would like to thank all contributors and authors of this book.

How to reference

In order to correctly reference this scholarly work, feel free to copy and paste the following:

N.I. Chkhalo, A.E. Pestov, N.N., Salashchenko and M.N. Toropov (2010). Manufacturing and Investigating Objective Lens for Ultrahigh Resolution Lithography Facilities, *Lithography*, Michael Wang (Ed.), ISBN: 978-953-307-064-3, InTech, Available from: <http://www.intechopen.com/books/lithography/manufacturing-and-investigating-objective-lens-for-ultrahigh-resolution-lithography-facilities>

INTECH

open science | open minds

InTech Europe

University Campus STeP Ri
Slavka Krautzeka 83/A
51000 Rijeka, Croatia
Phone: +385 (51) 770 447
Fax: +385 (51) 686 166
www.intechopen.com

InTech China

Unit 405, Office Block, Hotel Equatorial Shanghai
No.65, Yan An Road (West), Shanghai, 200040, China
中国上海市延安西路65号上海国际贵都大饭店办公楼405单元
Phone: +86-21-62489820
Fax: +86-21-62489821

© 2010 The Author(s). Licensee IntechOpen. This chapter is distributed under the terms of the [Creative Commons Attribution-NonCommercial-ShareAlike-3.0 License](#), which permits use, distribution and reproduction for non-commercial purposes, provided the original is properly cited and derivative works building on this content are distributed under the same license.

IntechOpen

IntechOpen